

EXPERIMENTAL INVESTIGATION OF EFFECT OF SUPPORT STRUCTURE  
GEOMETRY ON THE MICROSTRUCTURE AND METALLURGICAL PROPERTIES OF  
IN718 PARTS FABRICATED BY SELECTIVE LASER MELTING

by

SOURABH HEMANT THAKARE

Presented to the Faculty of the Graduate School of

The University of Texas at Arlington

in partial fulfillment of the requirements

for the degree of

MASTER OF SCIENCE IN MECHANICAL ENGINEERING

THE UNIVERSITY OF TEXAS AT ARLINGTON

August 2020

Copyright © by Sourabh Hemant Thakare 2020

All Rights Reserved



## **Dedication**

“Nothing can be compared to what we came through”,  
To my source of motivation, my mother, Anita Thakare.

## **Acknowledgement**

I would like to show my deepest gratitude to my supervising professor Dr. Amir Ameri for his immense patience, encouragement, support and guidance throughout my graduate studies. I would also like to thank Dr Narges Shayesteh for her valuable guidance. Without their supervision and efforts this thesis would not have been possible.

I would like to thank Dr Ankur Jain and Dr Raul Fernandez for providing their invaluable time to serve on the thesis committee. Along with this, I appreciate the Characterization Center for Materials and Biology at the University of Texas at Arlington for allowing us to use their resources for the experiments.

I would like to thank my dear lab members at IAM lab and AMERI lab for their assistance. Mr. Bharath R, Mr. Kiriti M, Mr. Behzad F, Mr. Srihari S, Mr. Vignesh R, Mr. Himanth T and Ms. Behnaz H for playing an instrumental role in completion of the thesis and making this journey memorable.

I want to thank my mother, Ms. Anita Thakare, my sister, Ms. Mayuri Thakare, and my uncle for their support and belief in me, and my friends Ms. Sayali Throat and Mr. Venugopal Yadav for taking care of my family during my absence. Finally, I would like to express my respect and my love towards the ones who could not be here today, my father Mr. Hemant Thakare and my grandmother Mrs. Sushila Mohod.

**Abstract:**

STUDY ON EFFECT OF SUPPORT STRUCTURE GEOMETRY ON THE MICROSTRUCTURE  
AND MECHANICAL PROPERTIES OF IN718 PARTS FABRICATED BY SELECTIVE LASER  
MELTING.

Sourabh Hemant Thakare, MS

The University of Texas at Arlington, 2020.

Supervising Professor: Dr. Amir Ameri.

Additive manufacturing is a modern manufacturing technique that provides extreme design freedom and the ability to manufacture multiple parts with high complexities at the same time. Various fabrication techniques have been developed, and this study focuses on selective laser melting (SLM) due to its ability to provide near-perfect parts at low cost while being able to work with a wide range of materials. In SLM, the part is manufactured, layer-by-layer, by melting and solidification of powder material under controlled inert conditions.

The fabrication of complex geometries is not possible without proper allocation of support structures for the part, which keeps the component intact and retains structural stability while manufacturing. The main function of the support structure is to complement the fabrication of the main part and reduce the chances of abnormalities in the structures or complete failure of the fabrication process. Supports are attached to the part and are to be removed after fabrication in such a way that the required surface finish is not compromised. Multiple properties like microstructural composition, residual stresses, mechanical properties, hardness, and toughness of SLM parts are either directly or indirectly affected by the allocation of a specific type of a support geometry. The challenge is to identify and allocate appropriate support structures after analyzing the part and the part orientation while ameliorating the functionality of removability, reducing material consumption, and enhancing structural support.

IN718 is a type of high-strength corrosion-resistant super alloy, which consists of nickel and chromium. It can withstand extremely high pressure and heat, which makes it suitable for high-end applications such as aerospace and petroleum. Due to the high toughness of the superalloy along with its work hardening, the difficulty in machinability of IN718 is immense, and thus the adaptation of additive manufacturing, specifically SLM, comes into consideration.

This study focuses on the effect of support structure geometry on the surface topography along with composition, hardness, melt-pool size, and grain structure for IN718 parts after the fabrication and removal of multiple iterations of support structures. A comprehensive report on the effect of support structure design is provided after studying the fundamental parameters of design, fabrication, testing, and results interpretation for the IN718 parts.

## Table of Contents

Dedication .....	iii
Acknowledgement .....	iv
Table of Contents .....	vii
List of Tables .....	ix
List of Figures .....	x
Chapter 1. Introduction .....	13
1.1. Motivation.....	13
1.2. Objectives .....	13
1.3. Approach.....	14
1.4. Outline.....	14
1.5. Contribution .....	15
Chapter 2. Background and literature review .....	16
2.1. Additive Manufacturing processes.....	16
2.1.1. A brief history of additive manufacturing development.....	16
2.1.2. AM technologies.....	17
2.1.3. Effective parameters on AM processed part .....	23
2.1.4. Advantages and disadvantages of AM.....	28
2.1.5. AM applications.....	29
2.2. AM of Inconel718 superalloy .....	30
2.2.1. Brief introduction to Inconel718 superalloy .....	30
2.2.2. SLM of IN718.....	32
2.3. Support structures in AM.....	33
2.3.1. Importance of supports in SLM .....	34
2.3.2. Principle of support design .....	35
2.3.3. Cost of estimation for support structures .....	36

2.3.4. Support structure generation software for SLM .....	37
2.3.5. Types of support strategies .....	38
2.3.6. Metrics of optimizing support structures .....	39
2.3.7. Support Structure optimization .....	40
Chapter 3. Design, fabrication and experimental procedures .....	44
3.1. CAD design.....	44
3.2. Support preparation.....	44
3.3 Powder preparation and fabrication .....	46
3.4. Sample preparation .....	47
3.5. Experimental procedures.....	49
3.5.1. Scanning electron microscopy (SEM) and Energy Dispersive X-Ray Spectroscopy (EDS)....	49
3.5.2. X-Ray diffraction (XRD).....	50
3.5.3. Hardness analysis.....	51
Chapter 4. Results and discussion.....	52
4.1. Fabricated samples .....	52
4.2. Microstructure analysis .....	52
4.3. Compositional Analysis .....	59
4.4. Hardness analysis .....	63
4.5. Build time and material cost estimation.....	65
Chapter 5. Conclusions and Future Works .....	67
5.1. Conclusion .....	67
5.2. Future Work .....	68
Reference .....	69

## List of Tables

Table 1. Main features of available laser-based powder bed AM processes. ....	19
Table 2. Composition of IN718 (wt%) [108]......	31
Table 3. Variation in cost models, which include sub-factors as follows, based on literature review.....	37
Table 4. different types and geometrical factors (G and T) for support structures. ....	46
Table 5. Effect of support structures on the melt pool size and grain structure on the side of the fabricated part near the support zone. ....	58
Table 6. Calculation of % area of phases for the fabricated IN718 sample on top of different support structures (With the intention of eliminating noise in the system, a minimum intensity value is kept for all graphs. Peaks with values more than the minimum intensity are detected, and the areas are represented.) .....	61
Table 7. Hardness values on the bottom side of all main parts facing support structures .....	64
Table 8. Calculation for build time and support volume for all supports geometries.....	66

## List of Figures

Figure 1. Different types of AM processes: liquid-based, solid-based, and powder-based differentiated according to the feedstock material type.....	18
Figure 2. A schematic of a SLM system. This procedure starts with slicing the CAD model and continues with a repeatable three-step process. Where step one is to elevate the powder platform, step two is to spread powder, and step three is to melt powder according to the CAD file, and the cycle is repeated over. After the supports and loose powders are removed, the final product is ready to use. ....	20
Figure 3. The effect of indirect SLS process on metal powder particle. In the first figure, the loose powder with a polymer binder is contained. The powder is fused, and the part takes shape without affecting the metal powder. The next step talks about how, after heating, the polymer gets vaporized and leads to a porous part. To decrease the porosity, a metal powder with a lower melting temperature is added, which fills up the gaps [4].....	21
Figure 4. Stochastic exposure strategy in Laser curing process. ....	23
Figure 5. Hatch angle: 90 degree (left) and 67 degree (right).....	25
Figure 6. The schematic of the staircase effect in layer-based manufacturing processes(left); and the technique to minimize the staircase effect (right) [80]. ....	26
Figure 7. Balling effect in the fabrication cycle, which occurs when energy for melt pool is too small or the laser melting time is less [87]. ....	28
Figure 8. Parallel scanning (a) in one direction, and (b) with a change in direction at alternate scan; (c) scan strategy with several small islands.....	28
Figure 9. Jet engine bracket for aerospace applications (left) [99]; OEM brake caliper for automotive application (right) [100]; world’s first 3D printed heart with functional heartbeats in medical applications (bottom) [101].....	30
Figure 10. Super-alloy material in a wrought form (left), casting, and powder (middle) and AM (right)[109]. .....	31

Figure 11. a) 3D systems 3DXpert [143]; b) Materialize Magics [144]; c) Atlas3D Sunata [145]; d) Siemens NX [146].	38
Figure 12. Different types of supports for SLM including a) block support; b) point support, c) web support, d) contour support, and e) line support g [147].	38
Figure 13. (a) bio-mimics support structures including honeycomb [148]; (b) Fractal used in SLM [149].	39
Figure 14. (a) Fabrication of ‘T’ part needing more supports, (b) Orientation shifted by 90° and is requiring lesser supports. (c) Elimination of supports by changing part orientation [126].	40
Figure 15. Reduction of critical angle using external features, leading to the elimination of support requirements.	41
Figure 16. Support generation flowchart explaining step by step procedure for modeling of an optimized support structure [156].	43
Figure 17. Main fabrication Sample Setup{Thakare, 2020 #163}	44
Figure 18. CAD designs of different support structures a) angled; b) cone; c) pin; d) concentric types; e) magics type.	44
Figure 19. Top view of the grid support structure (left); concentric support structure (right). The thickness of the support wall is presented as “T” and the gap between the neighbor wall is shown as “G”.	45
Figure 20. EOS M290 metal 3D printer with a fiber 400 W laser.	47
Figure 21. Allied Techcut 4™ Precision Low Speed Saw used for cutting.	48
Figure 22. Schematic of separation of the support structure and main part. Also, the cut section of the main part is presented. XRD analysis was conducted on the bottom surface of the main part. The SEM images from the main part were taken from the polished side surface.	48
Figure 23. Allied E-PREP 4™ Grinder/Polish.	49
Figure 24. Hitachi S-3000N Scanning Electron Microscope.	50
Figure 25. Bruker D8 Advance X- ray diffractometer.	51
Figure 26. LECO LM 300 AT Micro Hardness Tester	51

Figure 27. SLM IN718 samples with different support structures fabricated on a stainless-steel building plate..... 52

Figure 28. (a) SEM micrograph; (b) particle size distribution for commercial EOS IN 718 powder..... 53

Figure 29. (a) SEM of fresh IN718 powder; (b) table describing percentage composition for each element; (c) EDS compositions of IN718 fresh powder tested..... 54

Figure 30. SEM images of melt pool size for 1) angled (thickness=0.33; gap=1); 2) angled (thickness=0.53 ; gap=0.8); 3) cone (thickness=0.33; gap=1); 4) cone (thickness=0.53; gap=0.8); 5) pin (thickness= 0.53 ; gap=0.8); 6) T variation (thickness= 0.8; gap=0.8); 7) T variation (thickness=0.35; gap=0.8); 8) T variation (thickness=0.6; gap=1); 9) G Variation (thickness=0.33; gap=0.81); 10) G Variation (thickness=0.33; gap=1.27); 11) G Variation (thickness=0.53; gap=0.61); 12) G Variation (thickness=0.53; gap=1.07); 13) Concentric ( thickness=0.5; gap=0.8) 14) Concentric (thickness=0.45; gap=1) 15) Magics (thickness= 0.33 ; gap=1). ..... 57

Figure 31. XRD image of fresh powder and 15 samples. .... 60

## **Chapter 1. Introduction**

### **1.1. Motivation**

SLM is one of the most widely used metal Additive Manufacturing (AM) techniques for IN718, and for the fabrication of almost all complex geometries, there is a mandatory need to include support structure to augment the main part fabrication. These support structures are basically essential sacrificial entities that help to fabricate the parts over the process. Supports not just help in keeping the structure intact and together, but it helps in reducing warping of thin parts, removal of heat due to the laser melting, etc. Due to the prominent role of supports in SLM, the effect of the structures on the part fabrication is mandatory.

Along with the assistance in manufacturing the parts, there is a considerable effect on the main part properties such as microstructural properties, mechanical properties, hardness, roughness, etc. Since these are sacrificial entities, the material, time required along with multiple factors like energy, argon gas, etc. leads to an increase in direct and indirect costs. Due to this reason, the optimal condition should be recognized, pinpointed, and implemented such that there is less consumption of these important economic factors.

### **1.2. Objectives**

This study basically focuses on the effect of various types of support structure geometry and the overall impact on the fabrication parameters like the economy, resources, energy consumption, material wastage, etc. Since all these factors are interrelated, a necessity to tweak the effecting parameters in order to obtain the best results is recognized. While a lot of research on optimization of supports and structures of the same has been conducted, minimal work on the effect of such different support structures on various parameters like hardness, microstructural composition, melt pool analysis has been done. In order to get an apparent idea of how support structure affects the main body and how the parameters can be tailored to meet the above-mentioned goals, the influence on the mechanical and structural properties for the part are investigated.

### **1.3. Approach**

A literature review was the first step in initiating this study and to understand the basic process and the important parameters for SLM manufacturing of IN718 parts, the importance of supports in SLM, types of support geometries, etc. After the literature review, a structured plan to model various support structures was prepared. Multiple iterations of the same parts with different geometric values were introduced to understand the effect of any single parameter for that very specific type of support geometry. The CAD designs were modeled on various different software like Solidworks, Magics, etc. EOS M290 machine was used to fabricate the parts, and after fabrication, the parts were carefully removed off the build bed. Supports were separated from the main part, and the parts were prepared for various tests like X-ray Diffraction (XRD), Selective Electron Microscopy (SEM), Vickers Hardness, etc. At every point in the process, utmost safety was observed, and proper recording and labeling of data were ensured. The rest results were interpreted, and the effect of the support geometries for IN718 parts was observed and recorded for scientific use.

### **1.4. Outline**

Chapter 1 talks portray a summary of the research along with acknowledgment to the scientific community and the members for their direct and indirect efforts.

Chapter 2 provides information on the background and literature review. Section 2.1 talks more about the material being used, i.e., IN718, history of the same, and its importance in the metal AM ecosystem. Subsection 2.2 talks on the history of metal AM and the factors affecting the SLM fabrication method, along with benefits and drawbacks. Details on supports and the importance can be obtained from chapter 2.3. Explanation on types of supports and the idea behind consideration of supports for the study can be obtained from this chapter.

Chapter 3 describes the CAD design of the part and the support geometry that is fabricated and the selection of supports for the study. A detailed explanation of the handling and preparation of powder metal

is explained in chapter 3.3. Different experimental procedures that are used in the study are described along with the details and settings in chapter 3.4.

In chapter 4, the final work of presenting experimental recordings and the interpretation for multiple criteria is described. Along with the results, pictures, and details of the part fabrication and support seriation is explained.

And finally, chapter 5 concludes the results with appropriate reasoning and talks on how this research can be used by the community to bring out the best for all.

## **1.5. Contribution**

Contribution of this research will be in-line to the following:

- (i) Determination of the microstructural effect of the support structure for IN718 parts by SLM fabrication.
- (ii) Determination of optimal support structure for best build and material properties for IN718.
- (iii) Investigation of results for variation in thickness of supports for parts manufactured by SLM.
- (iv) Investigation of results for variation in the gap between supports for parts manufactured by SLM.
- (v) Study and comparison of concentric type and block type supports SLM manufacturing of IN718 parts.
- (vi) Study and determination of effect on melt pool structure for support structure interface with the main part for IN718 samples fabricated by SLM method.
- (vii) Study and Determination of residual stresses for IN718 parts fabricated by SLM process with different types of support structures.

## **Chapter 2. Background and literature review**

### **2.1. Additive Manufacturing processes**

Additive manufacturing (AM) is a manufacturing technology in which products are built up layer by layer [1]. It is an additive process, in contrast to most current manufacturing methods, which are subtractive processes. AM is known under several different names, including 3D printing, additive fabrication, rapid prototyping, and rapid manufacturing. In the industrial market, AM is the preferred term for this technology. In recent years, AM techniques have been introduced as a promising method to produce complex metallic parts (e.g., porous scaffolds, freeform surfaces, and deep slots) because they can overcome several common problems associated with conventional subtractive techniques. While AM provides a wide range of advantages, multiple challenges make them unfit for high-end real-life applications. Issues such as anisotropic mechanical behavior, inhomogeneity in microstructures, void formation in parts, small build volume, and concerns with food and drug administration (FDA) brings the need for a comprehensive research to obtain better results and make AM real-life application compliant [2-5] . Different types of materials are used in AM techniques, including powder, wire, and sheet. Powder-bed-based methods are only capable of using powder; however, the flow-based methods can utilize either powder or wire [1, 6, 7]. In sheet lamination techniques, the only material that is used is sheet. In this method only, the outer contours of parts are cut, and the sheets are cut and stacked or the other way around. Multiple iterations of processes revolving around sheet lamination techniques is based off build material and cutting strategies [8].

#### **2.1.1. A brief history of additive manufacturing development**

For the last 20 years, AM technology has been developed significantly. Deckard and Beaman, began working on a 3D printing technology for powder material in 1984, which consisted of a 100W YAG laser heat source [9]. After which, in 1986, the ‘Betsy’ machine was developed by Deckard. The research towards selective laser sintering (SLS) continued for which a patent was finally filed at the University of Texas at Austin [10, 11]. EOSINT M250 was launched by EOS for the direct metal laser sintering technique

(DMLS) in 1995. In 1997 EOS and 3D systems started working on SLS together [12], and eventually, 3D systems later obtained the right for SLS by acquiring the company that was holding the patents filed by Deckard [9]. Andersson and Larson patented Electron beam melting (EBM) in 2000 [13], after which Arcam brought it into the market in 2002 [14]. A collaboration was to existence when Hp and Stratasys came into an agreement for manufacturing a line of HP-brand 3D printers for Stratasys in January 2010 [15].

Apart from that, in 2004, Fab@home and RepRap were two open-sourced FDM 3D printers introduced by Cornell University and the University of Bath [16-18]. FDM was the basic implemented technique for earlier printers, but now due to the expiring patents, the focus tends towards SLA. Though the part fabricated by FDM are cheap, the mechanical properties and performance of the FDM-processed parts are not the best [19]. Although the cost for Laser-based printing operation is high, the parts provide some superior performance characteristics. High-end commercial printers usually come with software specially designed for the printer, which helps in slicing the 3D model and providing accurate commands to the machine. Stratasys (merged with Objet since 2013), 3Dsystems (bought Z-Corporation since 2011) offer the commercial 3D printers to the market [20].

### 2.1.2. AM technologies

Multiple iterations of 3D printers are available in the market, such as flow-based, powder-based, solid-based. Based on the properties of the fabricated parts, powder-based techniques tend to be the most promising field (Figure 1). Laminated object manufacturing (LOM) comes under the category of solid-based process, stereolithography (SL), and fused deposition modeling (FDM). leis in liquid-based and finally, selective laser sintering (SLS), laminated engineering net shaping (LENS), and electron beam melting (EBM) come under powder bed-based processes [21].

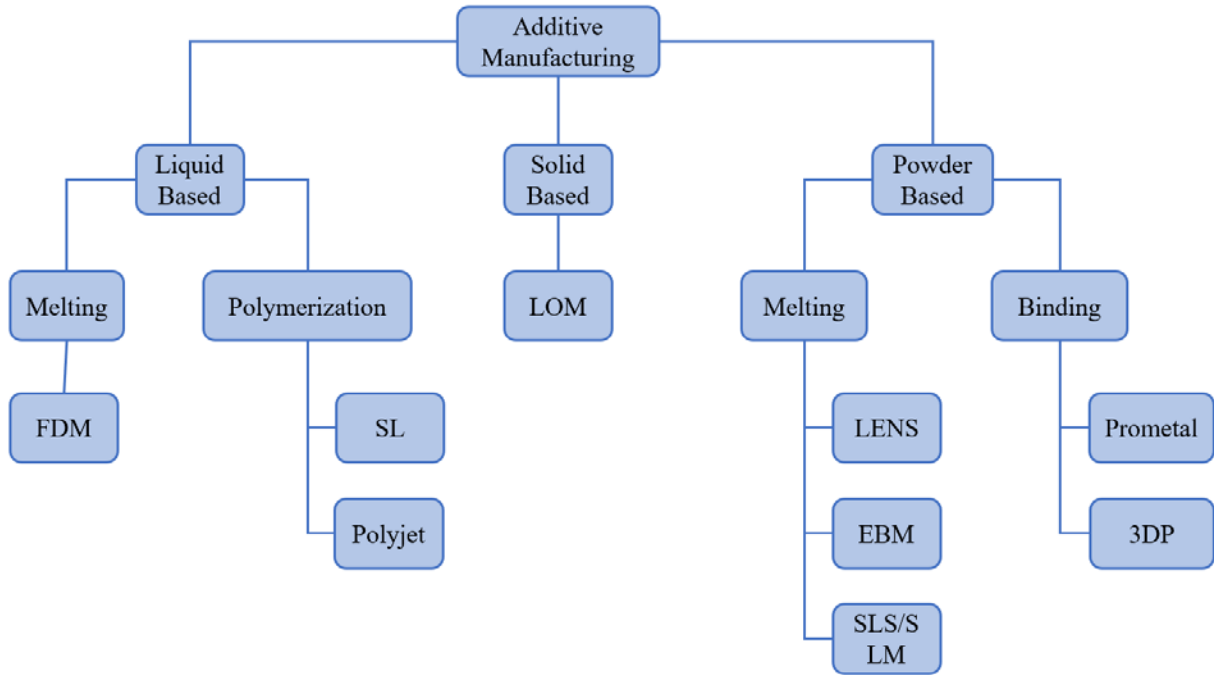


*Figure 1. Different types of AM processes: liquid-based, solid-based, and powder-based differentiated according to the feedstock material type.*

The majority of laser-based processes can be categorized into SLS, SLM, LMA, DMLS, LMS, and SLS/HIP. Several groups have implemented the above-mentioned AM techniques to produce parts for real-life applications. Table 1 briefly discusses several studies that have been conducted on laser-based AM. As it is presented over there, machine type, laser power, material, layer thickness, scanning speed along with other significant terms related to metal AM are discussed.

Table 1. Main features of available laser-based powder bed AM processes.

AM Technology	Machine Type	Laser Power (W)	Scanning Velocity (mm/s)	Hatch Space ( $\mu\text{m}$ )	Layer Thickness ( $\mu\text{m}$ )	Powder size ( $\mu\text{m}$ )	Author
SLM	-	110, 110, 120, 130	600, 400, 400, 400	-	-	15- 45	Jia <i>et al.</i> [22]
EBM	Arcam® EBM S12 machine	-	-	-	50	-	Raghavan <i>et al.</i> [23]
SLM	SLM 250HL machine	100 W	540	120	30	30	W.Tillmann <i>et al.</i> [24]
EBM	ARCAM A2 SEBM System	594 W	2200 to 8800	100, 37.5	-	-	Korner <i>et al.</i> [25]
EBM	EBM 12 SYSTEM FROM ARCAM AB	-	918	-	70	47 $\pm$ 23	Hinojos <i>et al.</i> [26]
SLM	Concept M2 machine	180-220	-	-	30 to 45	-	Lambert, Dennis M [27]
DLD	IPG Photonics 5 kW system equipped with an ABB robot	5000	-	-	-	-	Y.N.Zhang <i>et al.</i> [28]
SLM	SLM 280HL	250, 950	700, 320	120, 500	50,100	20 to 60	V.A.Popovich <i>et al.</i> [29]
LAM	-	550	-	-	-	-	Yuan Tian <i>et al.</i> [30]
SLM	DMP PROX300	450	1000 to 1800	50 to 90	70	5 to 25	K.Moussaoui <i>et al.</i> [31]
SLM	EOS M270	200	800 to 1200	-	-	-	Gangireddy <i>et al.</i> [32]

### 2.1.2.1. Selective laser melting process

Selective laser melting (SLM) has been recognized as the most promising AM technology due to its flexibility in feedstock and shapes. Complex components with high dimensional precision and good surface integrity can be obtained precisely by this process with no need for post-processing on fabricated parts, which the conventional methods cannot keep pace with easily [1, 33-37]. In SLM processes, a three-dimensional dense part is created directly from the user-defined CAD data through SLM of pre-spread powders in a layer-by-layer manner [38-44].

Figure 2 is presenting a schematic of a generic powder bed SLM system. The SLM process starts with raking powder across the work area. An energy source (electron beam or laser beam) is programmed to deliver the required amount of energy to the surface of the bed to melt or sinter the metal powder into the desired shape. Additional powder is raked across the work area, and the process is repeated to create a solid three-dimensional component. The advantages of SLM include its ability to produce high-resolution features, internal passages, and maintain dimensional control [45]. The desired microstructures of SLM-processed parts are inevitably affected by complicated physical and chemical behaviors within the molten pool, which often are the outcome of the non-equilibrium processing technique of laser [46].

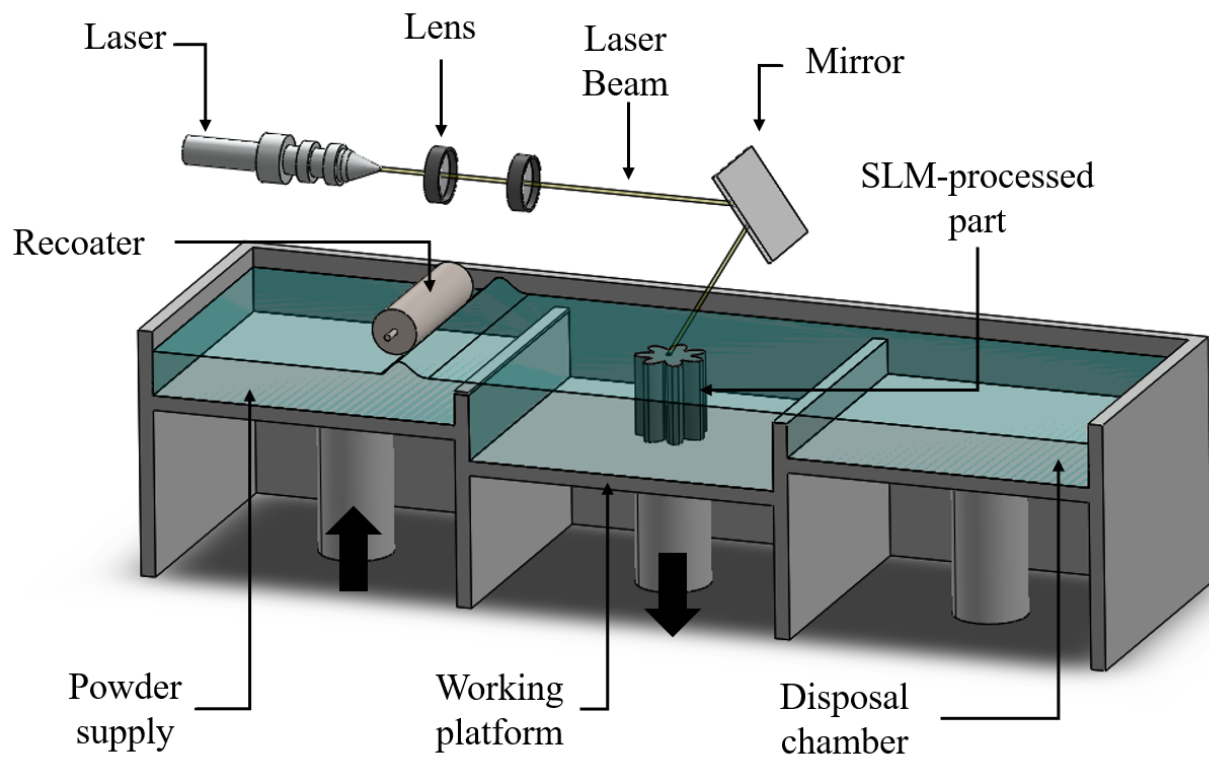


*Figure 2. A schematic of a SLM system. This procedure starts with slicing the CAD model and continues with a repeatable three-step process. Where step one is to elevate the powder platform, step two is to spread powder, and step three is to melt powder according to the CAD file, and the cycle is repeated over. After the supports and loose powders are removed, the final product is ready to use.*

### 2.1.2.2. Selective laser sintering

Direct and indirect are two predominant categories of selective laser sintering (SLS). Sintering means the fusion of powder particles without melting under high temperatures. In direct SLS, the powder melts partially and provides low packing density. Direct SLS provides a good enough sintering density but leads to cracks in part due to the thermal stresses. One practical approach is to preheat the powder bed by diffused CO<sub>2</sub> laser up-to 1700 °C. The maximum part height size is limited to 3 mm [46]. From Figure 3, in indirect SLS, the green part is obtained by the melting of a binder phase. After which the green part is then converted to ceramic by rebinding and then furnace heating. A major difference between direct SLS and indirect SLS is absence binder material in direct SLS [47].

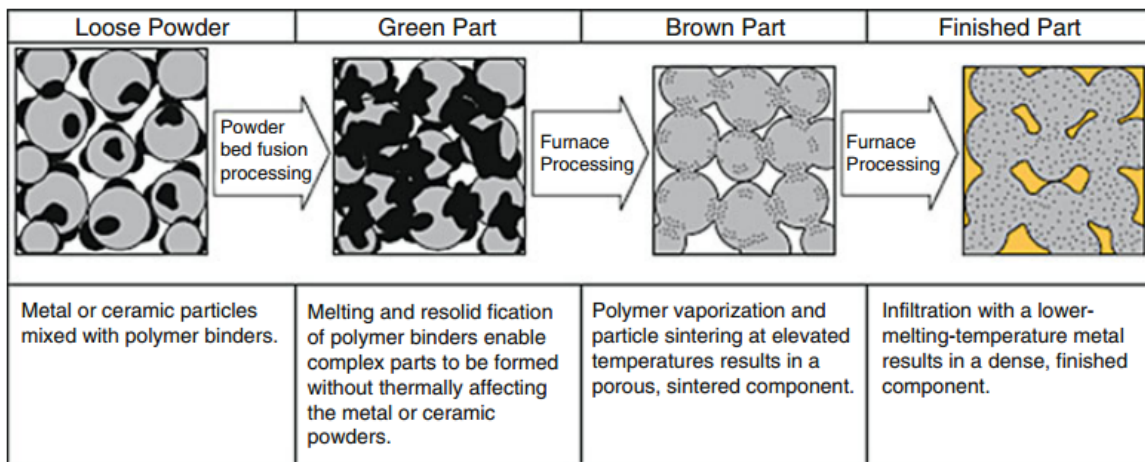


Figure 3. The effect of indirect SLS process on metal powder particle. In the first figure, the loose powder with a polymer binder is contained. The powder is fused, and the part takes shape without affecting the metal powder. The next step talks about how, after heating, the polymer gets vaporized and leads to a porous part. To decrease the porosity, a metal powder with a lower melting temperature is added, which fills up the gaps [4].

### 2.1.2.3. Direct metal laser sintering

Due to the recent development, the initial need towards binder for titanium and aluminum is eliminated, and the potential to build fully working metal prototypes has increased. Under a proper working condition, this method can fabricate parts with the same or almost similar properties of a conventionally fabricated part. The ability to build more complex parts in a single step turns out to be an advantage over

SLS but can provide the following disadvantages: (i) High internal stress and part distortion leading to an increase in temperature gradient and densification ratio. (ii) Bad surface finish due to balling and dross formation [48-50]. The surface finish of a part is critical in many applications, for example, those requiring a surface roughness of 0.8  $\mu\text{m}$  or better to avoid premature failure from surface-initiated cracking.

#### *2.1.2.4. Laser micro sintering*

Laser Institute Mittelsachsen eV introduced laser micro-sintering in 2003. This technique and the equipment were marketed by 3D-Micro-mac AG, Chemnitz, Germany, which provided a resolution of less than 30  $\mu\text{m}$  and lesser roughness ( $R_a = 1.5 \text{ V}$ ). The manufacturing process flow for laser micro sintering is similar to SLM, and it offers a better resolution compared to SLS (less than 100  $\mu\text{m}$  for parts) [51]. Another positive impact of this method is the minimal tension in the parts due to q-switched Nd: YAG-laser pulse [52].

#### *2.1.2.5. Laser cusing process*

Concept laser brought the concept of M1 cusing, M2 Cusing, M2 cusing multi-laser, and M3 linear machines. Cusing derives from the letter “C” and the word “Fusing”. A specialty of this method was the ‘stochastic exposure strategy’, where each layer is called as an island (Figure 4). This method leads to the reduction of internal stress for the fabricated part [53]. Usual layer thickness this method is 20 to 50  $\mu\text{m}$  [54]. The second generation of this technique developed by concept laser is M2 cusing. M2 cusing has a double-fiber laser-equipped, which causes a reduction in the fabrication time. The flexibility of material selection, including stainless steel and other chromium alloys, makes the M3 linear machine easier. The capability of processing nonferrous alloys, like titanium (Ti6AlV4), aluminum (AlSi12 and AlSi10Mg), and other cobalt-chrome and nickel-based alloys [54-63].

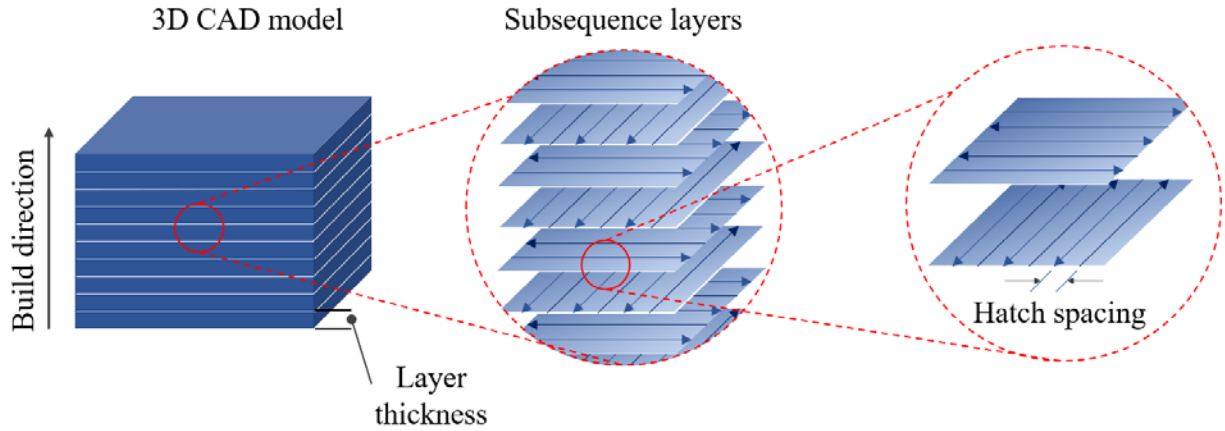


Figure 4. Stochastic exposure strategy in Laser cusing process.

### 2.1.3. Effective parameters on AM processed part

AM deals with the interpretation of interactions between multiple parameters, directly and indirectly, related to machine, materials. Parameters like powder particle size, scanning strategy, laser power, hatch spacing, etc. are to be altered and supplemented according to the part details.

Yadroitsev *et al.* [64] introduced process parameters differentiated as factors mentioned below: (i) Manufacturing strategy: part orientation, support strategy. (ii) Laser: laser power, spot size, scanning velocity. (iii) Powder-based: Powder size, shape, composition, and layer thickness. To summarize, the primary focus to optimize the part quality lies in factors like powder morphology, laser power, hatch size, layer thickness, scanning velocity, and scanning strategy. An optimal combination of these processes is necessary for SLM to fabricate a full-density sample [19, 65-75]. The laser energy density can be calculated by using Equation 2.1 from laser processing parameters:

$$\text{Laser energy density} = \frac{\text{Laser Power}}{\text{Scan Spacing} \times \text{Scan Speed} \times \text{Layer Thickness}} \quad \text{Equation 1}$$

Initial feedstock material affects the heat capacity and the latent heat. The issue of insufficient energy occurs when the combination of laser power, scanning speed, and layer thickness are subpar. This issue leads to balling phenomena, which is due to the wetting of the molten pool with respect to the other layer [76]. While low scanning speed and higher laser power lead to excessive material evaporation and key-hole effect [77]. Not just that, but poor hatch spacing leads to an increase in porosity of the parts.

Condensation of the volatilized material in the fabrication chamber causes the laser window to get blocked, which leads to an adverse effect on the laser power. The above parameters are affected due to vaporization in SLM [78].

#### *2.1.3.1. Powder particle morphology*

Irrinki *et al.* [78] found that density and mechanical properties of SLM parts get effected by powder atomization, particle size, and shape. Attar *et al.* [79] worked on understanding the effect of powder morphology on the density of in-situ Ti-TiB composite parts. To relate the density of samples fabricated by spherical and irregular particle shape as 99.5% and 95%, respectively.

#### *2.1.3.2. Laser power and spot size*

AM governs over the melting of feedstock material, which is affected by the property of laser power. With an increase in laser power, the process of melting of powder and powder properties are degraded. Hence, the optimal level of laser power is supposed to be determined, depending on the type of material. For polymers, 5W is enough, while in case of ceramics or metal, the power needs to be 500 W. Typically, commercial SLS or SLM machine is equipped with 50 to 400 W laser power. Another parameter to help decide the laser power is the laser spot size. With a decrease in laser spot size, higher laser density is attained and leads to adaptation towards use for materials with higher melting point [80].

The term for laser spot size is laser beam diameter. For a Gaussian wave, the point at  $e^{-2}$  for the laser peak intensity of a beam depicts the diameter of laser spot size. It affects energy density, precision, and production speed. Energy density is inversely related to the spot size. To understand the minimum spot size requirement, the wavelength, and the quality of the laser is to be assessed [81]. The use of small spot size for building thin walls and small holes is obvious. But this in-turn increases the build time, which is undesirable in some instances. Thus, for small features, thin boundaries are used, and for bulk production, larger spot diameter is used [80].

### 2.1.3.3. Hatch spacing

The separation between two tracks, called by multiple names such as hatch spacing, scan spacing, or hatch distance, can be measured by calculating the distance between the center of one beam to the center of the adjacent beam [80]. There is a direct relationship between the hatch spacing and the production speed. Less hatch spacing leads to lesser scanning time for the laser and vice versa. Another primary parameter is hatch angle  $\theta$ , which is the angle between the laser scanning direction amongst the consecutive layers. When the hatch angle is 90, the orientation of the melted rows after four layers will be the same, i.e., the same as the first layer [82].

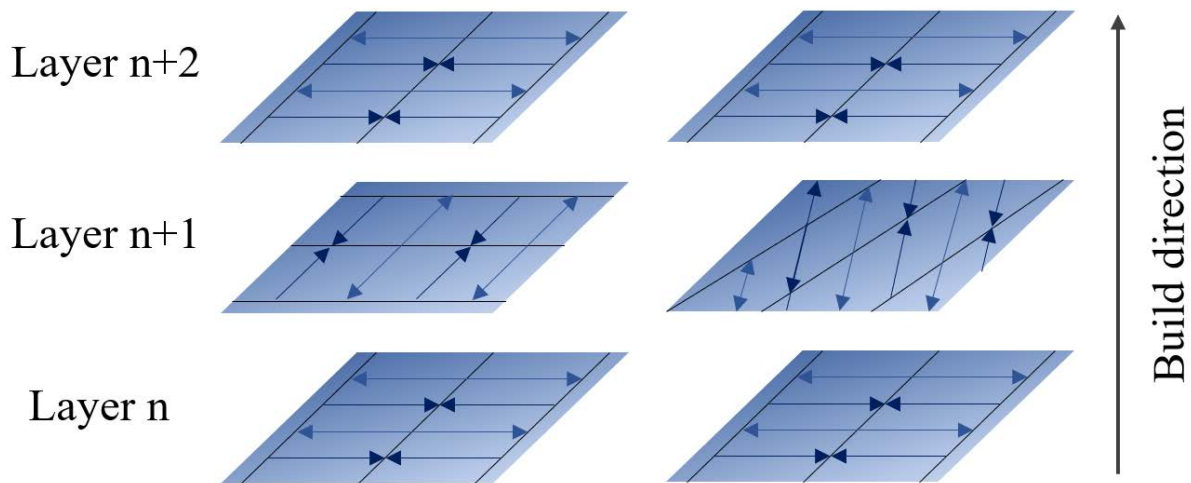


Figure 5. Hatch angle: 90 degree (left) and 67 degree (right).

### 2.1.3.4. Layer thickness

The thickness of a powder layer or thickness of a CAD slice is called a layer thickness. There is a direct proportionality between fabrication speed, build time, and layer thickness. But the quality of the AM-processed part decreases with an increase in the layer thickness. A thick fabrication layer in AM may lead to failure. Higher laser energy comes along with an increase in layer thickness. To increase the dimensional accuracy of the parts, thinner layers should be selected due to which there will be less shrinkage, distortion, within the layers. While there are some benefits to thin layers, there is a direct increase in build time and

build cost. In order to have better part properties for a thick layer, instead of using higher laser energy, two scans with lower energy should be preferred [80]

The thickness of a layer in AM depends on the topology of the sample. As it is shown in Figure 6a, curved object while being fabricated layer by layer, cannot be fabricated the same way, since there will be gaps on the sides of the part [80]. This effect is called the staircase effect. Thus, to eliminate unwanted features like the staircase effect, the layer thickness has to be optimized. Therefore, for vertical surfaces, the higher layer thickness can be allocated, but for surfaces with slopes, thinner layers are suggested, as explained in Figure6b.

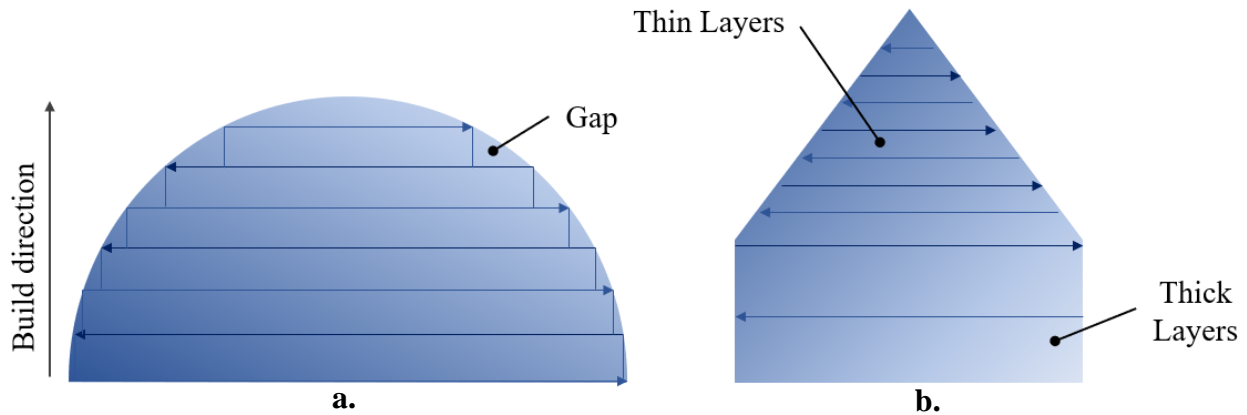


Figure 6. The schematic of the staircase effect in layer-based manufacturing processes(left); and the technique to minimize the staircase effect (right) [80].

#### 2.1.3.5. Scan speed

The speed with a laser beam scans a line is the scanning speed, and it affects the rate of the production, and it affects the production speed and building time. By increasing the scanning speed, the laser energy density decreases and thus is insufficient for the proper melting of the material. However, an increase in laser power will help compensate for the issue. Higher scan speed will not allow the layers to solidify before the next layer, and this affects the melt-pools. Higher scanning speed will lead to longer and

thinner melt-pools, which is not desired since the chances to break into smaller pools(balls) is high considering the theory of Rayleigh Instability (Figure 7) [80, 83].

#### *2.1.3.6. Scan strategy*

The method of scanning of powder bed with a laser beam for increasing the build speed and part quality is scanning strategy. The selection of an optimal scanning strategy leads to a reduction in distortion, warp, inaccuracy, and porosity [84, 85]. Fill scan and contour scan are two basic types of the scanning strategy. Infill scan the entire area is scanned, and in contour scan, just the boundaries are scanned. From Figure 8a, an understanding of fill scan and counter can be obtained. The fill scan covers the complete area in one scan direction. Another scanning strategy is described in Figure 8b, where the fill scanning has an alternating scan direction. The scan time presented in Figure 8b is less than the one in Figure 8a. This is because for Figure 8a, the laser has to go back to the starting point of the previous layer, unlike the other strategy where there is continuous scanning. For SLS/SLM, parallel lines scan modes are easy to program and implement. While the scanning can be horizontal and vertical, a consistent scanning angle can be allocated. A consistent scanning strategy leads to less shrinkage, residual stress, and anisotropy behavior [80]. Shrinkage stress can lead to a build of warping and distortion of the part [86]. The plane can be divided into smaller islands, as shown in Figure 8c, and this can decrease the anisotropic buildup. Thus, dividing and scanning the plane by islands reduces the problem of heat buildup from a bigger area (whole plane) to a small area (an island). Non-uniform heat distribution can be targeted by using different scanning strategies for different layers. Once an island is scanned, the next scanned island is at the opposite end of the plane to reduce the consequent build of stress, which leads to the warping of AM-processed parts, especially overhangs. Another additional factor is if the scanning path is bigger and thinner, the layer can break into several balls due to Rayleigh instability (Figure 7). Thus, a scanning strategy with several islands is a better choice [80, 83].

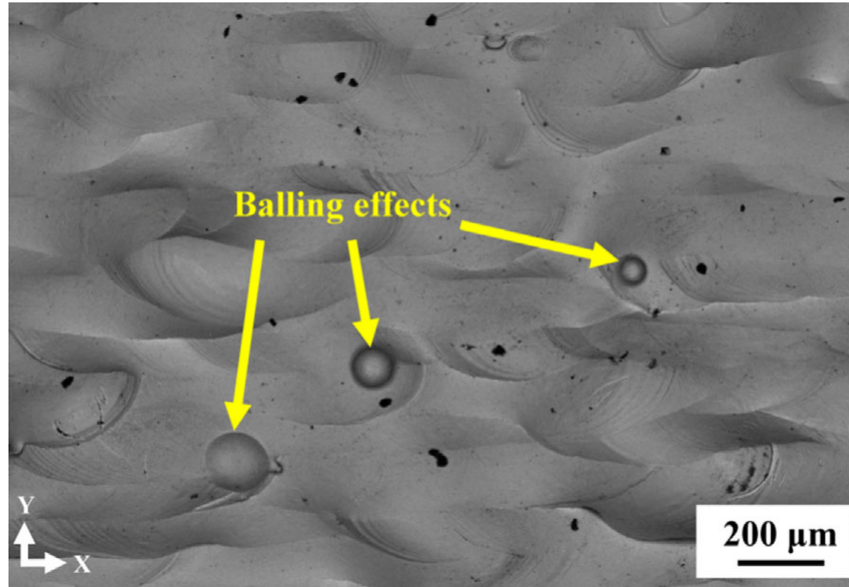


Figure 7. Balling effect in the fabrication cycle, which occurs when energy for melt pool is too small or the laser melting time is less [87].

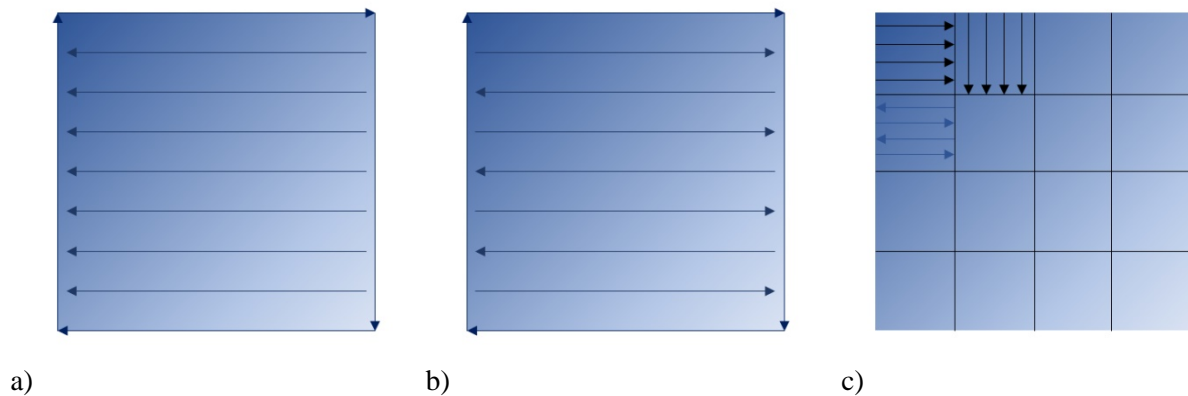


Figure 8. Parallel scanning (a) in one direction, and (b) with a change in direction at alternate scan; (c) scan strategy with several small islands.

#### 2.1.4. Advantages and disadvantages of AM

AM plays an essential role in the industry. Several factors, such as a reduction in build time, human interaction, and product development cycles, are some of the significant advantages along with unrestricted freedom to manufacture complex parts [88]. Due to an ever-increasing growth in the AM field, along with promising results and quick industrial adaptations, there is optimism in the technology securing an important place in the future of the manufacturing industry [21]. The eventual goal is to manufacture parts and prototypes for direct applications.

AM can have wide-scale adaptation in businesses when the cost of manufacturing, product development cost, cradle to grave costs, and others prove to be beneficial over a set of the product manufacturing cycle. AM has the vision towards the betterment of the economic, environmental, and experience value of the products. Ability to produce inhouse parts, maintain product security and privacy, though it cannot be directly quantified, but can help towards profitability [89-91]. The absence of a tool in AM leads to a reduction in direct production costs, in circumstances where the complexity of the part is high, and the production volume is low [92]. Thus, the fabrication time and time to market can be significantly reduced for such complex parts.

Just as a coin has two sides, along with multiple advantages, there are certain challenges associated with AM-processed parts, and there is a requirement for advancement in AM before they can be considered a standard in the manufacturing industry. One of those advancements is the elimination of the requirement of surface finishing. Due to the requirement of support removal, there is no consistency in the overall part surface finish. For high-end applications where the surface finish must be on-point, this is undesirable. Along with this, due to layer by layer building, the presence of the staircase effect leads to inconsistent and bad surface finish. These issues are to be brought into lime-light for the betterment of the properties.

At this moment, AM cannot be adapted in extreme high applications where the error percentage is required to be near to zero. Still, it can be noted that this technology is being widely adopted by scientists, medical doctors, students, artists, along with many others [93-95].

#### 2.1.5. AM applications

After intensive research, evidence on a significant amount of progress can be concluded with an increasing amount of applications in and not just restricted to aerospace, automotive, academics, biomedical, energy [96]. Alternative uses like the creation of structural plans for architecture, prototypes of jewelry, and fashion. The influence of 3D printing can also be seen in the food industry [97]. Not just this, but the patient-specific models of the damaged body parts, understand the anatomy and then plan the operation accordingly. Artists use AM to create a scaled model of their art [2]. Aerospace and automotive

manufacturers are using 3D printing on a major scale due to the freedom to manufacture complex parts while AM is associated with the medical field in a way where 3D printing of stem cells has been recently introduced and is being developed [98]. Several industrial applications of AM are presented in Figure 9.

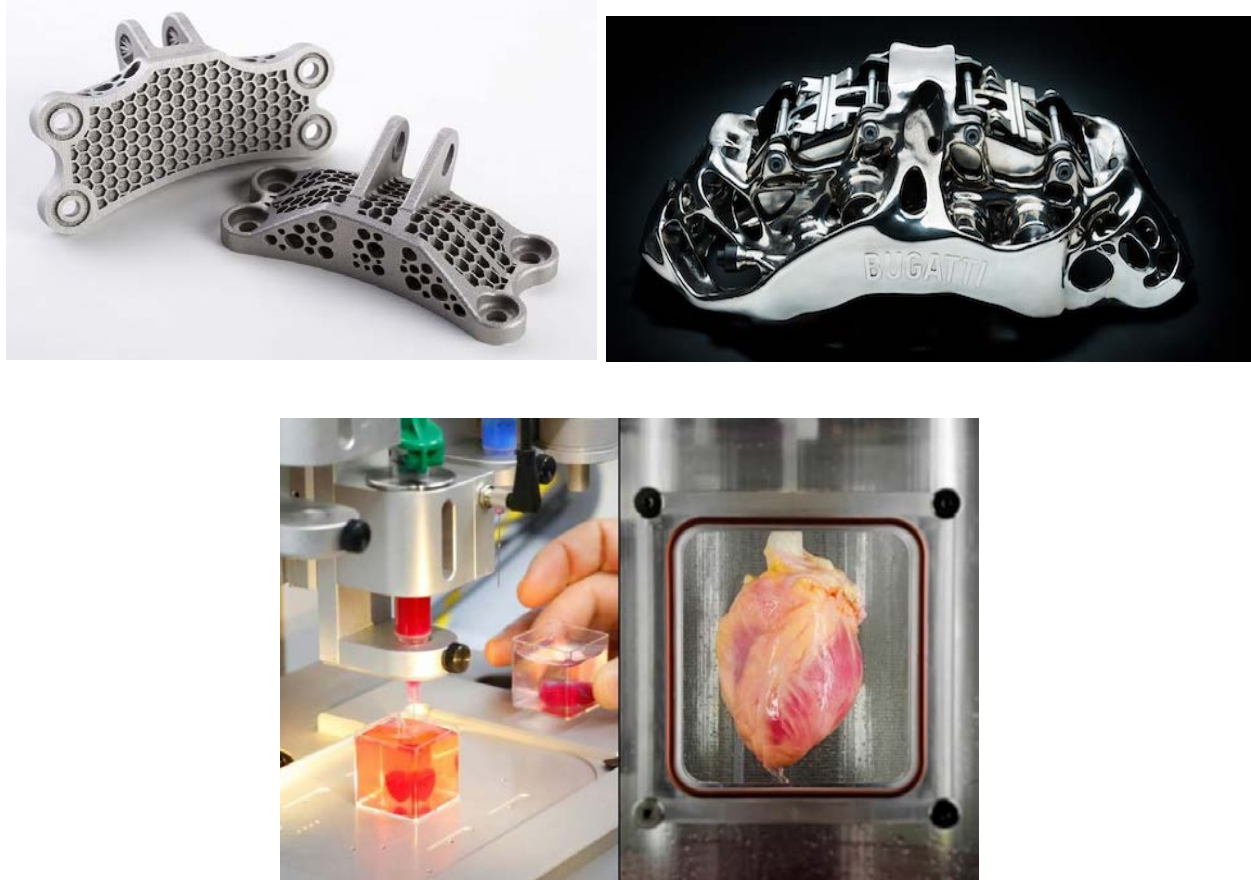


*Figure 9. Jet engine bracket for aerospace applications (left) [99]; OEM brake caliper for automotive application (right) [100]; world's first 3D printed heart with functional heartbeats in medical applications (bottom) [101].*

## **2.2. AM of Inconel718 superalloy**

### **2.2.1. Brief introduction to Inconel718 superalloy**

The need for a stable solution strengthened non-hardenable alloy for high-end applications at 1200 to 1400°F (650 to 760°C) led to the foundation towards the development of Inconel718 (IN718). In the earlier stages of development for Ni-based superalloy, stability was considered to be an important requirement. It was necessary to maintain the standard, for which the use of screening tests to check the

age-hardening response and metallurgical stability were introduced. After a while, the search was satisfied with the development of IN718 superalloy. IN718 superalloy is an age-hardenable Ni-Cr austenitic material with a wide service temperature ranging from  $-257\text{ }^{\circ}\text{C}$  to  $704\text{ }^{\circ}\text{C}$  [102, 103]. The development IN718 began from 1960 with a vision of combining better mechanical properties, creep-rupture strength, resistance towards chlorine and sulfide stresses and corrosion, extreme temperature resistance, oxidation resistance, welding characteristics, post welding cracking resistance, making IN718 one of the most widely utilized Ni-based superalloy. By these properties, IN718 can be used for applications such as aircraft engines, turbine blades, combustion chambers, and nuclear reactors [104-107]. The chemical composition of commercial IN718 is presented in Table 2.

Table 2. Composition of IN718 (wt%) [108].

Element	Wt%
Nickel	50.00-55.00
Chromium	17.00-21.00
Iron	Balance
Columbium	4.75-5.50
Molybdenum	2.80-3.30
Aluminum	0.20-0.80
Titanium	0.65-1.15
Manganese	0.35 max.
Silicon	0.35 max.
Boron	0.006 max.
Carbon	0.08 max.



Figure 10. Super-alloy material in a wrought form (left), casting, and powder (middle) and AM (right)[109].

Wrought, powder cast, metallurgy are some general forms of the superalloy. They can provide sufficient enough mechanical and microstructural properties [110-112]. Different methods of fabrication of IN718 are presented in Figure 10. This material offers superior mechanical properties for a wide range of temperatures, due to the solid-solution strengthening and precipitation strengthening. Meanwhile, conventional machining of IN718 is challenging due to high-hardness (372 HV for wrought IN718 based on AMS 5663 and 350 HV for cast IN718 based on AMS 5383) and low thermal conductivity ( $11.2 \text{ W}\cdot\text{m}^{-1}\cdot\text{K}^{-1}$ ) which will lead to extreme tool over-wear and unsatisfactory workpiece surface integrity [113]. Due to the major advantages and superior properties, high dimensional precision can be obtained, and thus the demand is higher [114, 115]. Though the pros for such material are high, a need for a non-traditional method of manufacturing comes into action, and thus AM has a prominent stand in this situation [46].

Generally, Nickel-base superalloys are the natural candidates for AM for both SLM and EBM processes. This situation arises due to the difficulties and limitations of conventional manufacturing methods, e.g., segregation, poor workability, machining cost. By now, Ni superalloy material that is being manufactured by SLM includes IN718, IN625, Hastelloy C, Nimonic 263, and others, which has a low concentration of Ti and Al. Other such materials that are being tested and applied are IN939, IN100, IN738LC, CM247LC, and Rene 142. SLM research has shown some great potential to be adapted in the standard manufacturing industry for the fabrication of complex geometry in minimal time and best properties [116].

### 2.2.2. SLM of IN718

SLM being recognized as a promising non-conventional AM technique and extreme flexibility in the selection of feedstock, shape, geometry, and obtain high precision and surface integrity. Depending on the application, SLM of Ni-based superalloys, are majorly applied in aircraft engines as swirlers in combustion chambers, which help in reducing smoke production and stabilizing the flame. It is also applied in repair patches, gas turbine blades, and turbo-charged rotors [117-119]. Great corrosion resistance, along with strength at high temperature, fatigue resistance, wear resistance, and good weldability, are just some

advantages [115]. Lu *et al.* highlighted in their review that Fraunhofer ILT and the MCP company had used SLM to produce complex turbine blades with high surface quality and dense microstructure [120].

Multiple variations in microstructure, hardness, mechanical properties can be obtained by SLM, let alone by different manufacturing methods [116]. Nuclear reactors and liquid-fueled rocket applications are possible due to excellent creep properties, good tensile strength, rupture strength, etc. [121]. Along with which excellent oxidation resistance and hot corrosion resistance have made it suitable for working at conditions where the temperature is 700 °C and conditions are extremely carburizing and oxidation [104-106]. Thus laser-based AM technologies have great applications for IN718 in the manufacturing industry with aerospace as a focus [122].

However, there are several challenges with the fabrication of IN718 through the SLM technique. It has been reported that there is a certain percent of porosity in the IN718 SLM-processed part (relative density 98.4%) [46]. Not just that, but some other problems are un-melted powder contents [123]. Hot isostatic pressing (HIP) can solve these issues to a certain extent, but the grain size will coarsen as well [124]. To have successful fabrication, an understanding of powder bed fusion limiting factors should be looked into to e.g., production quality and component dimensions [125].

### **2.3. Support structures in AM**

In powder bed fusion fabrication, the supports are used to build the parts and conduct energy from the molten pool to the build plate, which helps in providing stable thermal conditions for the process. Jingchao Jiang *et al.* [126] worked on understanding the significance of support structures in AM and suggested it to be an important parameter for a successful print. Supports reduce deformation in the parts with additional functions like the removal of heat and provide support to the sample fabrication. The basic requirement is that the minimum distance between the support structures should be such that the solidifying layers should not sink. While the dense concentration of supports will lead to longer build time, along with difficulty in support removal from the part and build platform [127].

him[127]. For which, alteration in support volume, density, and the production time should be the dominating parameters to obtain optimal results.

### 2.3.1. Importance of supports in SLM

Effective parameters related to production and removal of support structures in AM have been reported as being material consumption, energy usage, and manual post-processing by Jingchao Jiang *et al.* [126]. These issues are acknowledged as a minor inconvenience for the manufacturing of the prototypes. But the number of benefits of rapid prototyping; in this case, SLM outweighing the generic disadvantages.

In SLM research, numerous attempts are dealing with the fundamental development of strategies to avoid tension and deformation in the component. The exposure strategy plays a role in stress development in a sample. Kruth *et al.* [128]. By pre-heating the build plate, there is an increase in temperature gradient and thus can potentially solve the problem. By opting for this procedure, the microstructure and strain in the samples can be significantly reduced. While the number of defects can be reduced, the study of support structures and their optimization provide the best potential to receive the best possible parameters. The orientation and distribution of support structure with respect to the part will play an influence on the levelness of the build of parts, as observed by Gan and Wong *et al.* [129]. While some support strategy, when applied to a specific scanning strategy, will lead to a significant effect on the creation of pores within the initial layers.

Although the supports are sacrificial, they are considered to be a necessary function in the SLM process, and good design practice will help minimize them, as a lot of material and energy consumption factors are dependent on them. Still, they are also used to fulfill the following important functions [130] like to raise the part off the platform for easy removal, anchoring the overhanging and floating sections introduced during the build to the platform [131], strengthening thin-and-tall part during the build. These functions help prevent the toppling and destruction of the part by the forces of recoater, preventing part curling or distortion resulting from thermal stresses by dissipating heat away from the newly melted surface and ensure regular thermal conditions in the consolidation zone [132].

Along with multiple benefits, various factors help us understand the effect of geometry on the production ecosystem, such as internal stress, mechanical properties, material consumption, detachment of part from building plates, the maximum height of a manufactured part with overall aspects [133]. To decrease unwanted influences on the main part structure and properties, the manipulation in the geometrical design of a support structure could be considered as a parameter. The geometry acts as an influence on the manufacturability of part. The geometry also affects the support removal and surface roughness of the sample. The effect of support structures on material usage, build time, support removal time, residual stresses were studied and acknowledged by Papadakis *et al.* [134]. Excessive supports lead to an increase in material usage, build time, removal, etc. They have represented how weak supports will lead to failure of part production [130].

Several studies have been published regarding optimizing support structures for AM by reducing support materials and eventually reducing print time, and energy cost [129, 132-134]. However, to our knowledge, there is no unique study to discuss the effect of support structures in SLM on microstructure and composite of the fabricated part. To this end, a need to research and understand the influence of these supports is required [126].

### 2.3.2. Principle of support design

For a successful support design, based on literature, the following rules should be considered:

- (i) Avoiding large overhanging angles
- (ii) Avoiding printing large holes that are parallel to the printing surface
- (iii) Keeping access to holes where material can get stuck and has to be removed
- (iv) Reduction on support weight/ volume should be followed [126].

Due to the regulations on the main part after the fabrication cycle, the freedom to build an object by following the above rules could be limited. The parameters are supposed to be set based on the situations and the required output. Thus, before selecting supports for fabrication, factors such as printability,

overhang angle, thermal conditions, ease of removal with many others are supported to be considered [126]. Generally, the design of support structures should be based on basic principles such as (i) The strength between support and main part along with contact area between them should be minimum to assist in easy removal. (ii) Material consumption and build time should be considered as a vital factor in having a better print. (iii) Supports should have enough strength to prevent the part from collapsing or warping, and also the fabrication should be planned in such a way that the internal stresses are minimum. By following these principles, the potential fabrication and process issues can be eliminated, and the best possible version of the main part properties can be obtained [126].

### 2.3.3. Cost of estimation for support structures

The cost of AM is often viewed as one of the biggest barriers to adapt to the industry. However, there are many examples where a value-added by AM far outweighs the costs. This section explores the costs and economic benefits of AM-based production as barriers, motivations, and considerations for a design for AM. It presents some of the major cost models that have been developed for AM, considers the requirements for successful AM business models, and presents a series of case studies that explore the economic viability of design for AM.

Thomas *et al.* express AM costs as usually divided into well-structured direct production costs (e.g., labor, material, and machine costs) and ill-structured costs (related to building failures, transportation, and inventory) [135]. Traditional cost models focused on the well-structured costs and were intended to compare AM processes to each other or conventional manufacturing processes (wrought or casting). More recent works have attempted to evaluate the costs and economic benefits of AM by considering all life cycle costs, including the ill-structured costs [91, 136, 137].

Table 3. Variation in cost models, which include sub-factors as follows, based on literature review.

labor	Cost model							Author
	Pre-processing	Post-processing	Material cost	Machine cost	Electricity	Argon	Time	
✓	✓	✓	✓	✓	✓	✓	-	Li <i>et al.</i> [138]
✓	-	-	✓	✓	✓	-	-	Allen <i>et al.</i> [139]
✓	-	-	✓	✓	✓	-	-	Baumers <i>et al.</i> [140]
✓	✓	✓	✓	✓	✓	-	-	Gibson <i>et al.</i> [141]
✓	✓	✓	✓	✓	✓	✓	✓	Rickenbacher <i>et al.</i> [142]

#### 2.3.4. Support structure generation software for SLM

Depending on the application, the part and the objective, different support generation software are available in the current market to get the desired results. Companies like Materialize, Atlas3D, 3DSystems, Autodesk, Dyndrite, and Siemens have their version of AM support generation software in the market. Depending upon the application and the machine, appropriate software can be selected to generate the required support structure. The main part is imported in the software, and either manual or automatic support allocation can be used to get the final design, which then is submitted for printing. For the implementation of some design, porosity software like 3Matics (Materialize, Leuven, Belgium) is used. Along with this, various software such as Ansys Additive Suite (Canonsburg, Pennsylvania, USA), Simufact Additive (Hamburg, Germany), Autodesk Netfabb (California, USA) provides simulation for powder bed fusion processes, pressurization, heat treatment, support removal, shrinkage, warpage, residual stresses. Utilization of simulation softwares before the fabrication will lead to a reduction of part failures and wastage. Therefore, to get accurate results, we need to investigate the compatibility of the machine and the requirement of the supports to select appropriate software. Most commonly used software interfaces are displayed in Magics, Sunata, 3DXpert, and Siemens (Figure 11).

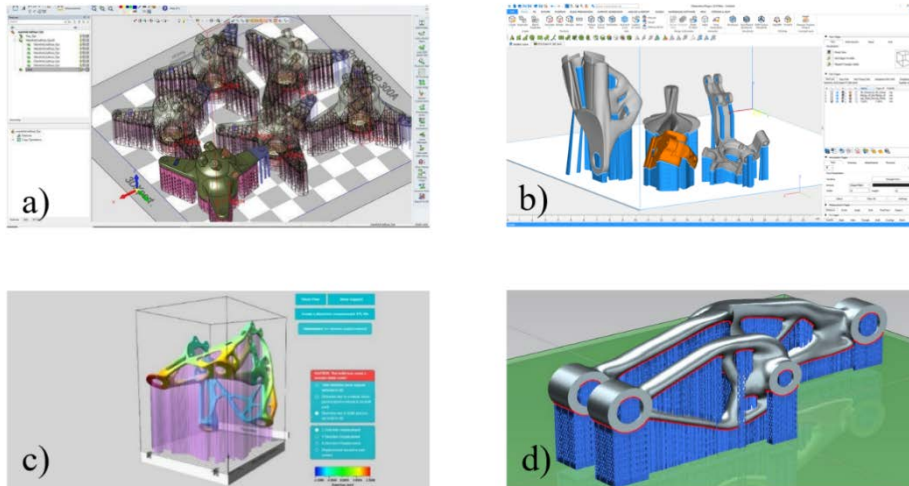


Figure 11. a) 3D systems 3DXpert [143]; b) Materialize Magics [144]; c) Atlas3D Sunata [145]; d) Siemens NX [146].

### 2.3.5. Types of support strategies

The degree of design freedom for modeling support is immensely resulting in a complex operation. Various software are used to generate different types of supports for the main part. Materialize Magics has a prominent standing in market as an STL editor. Majority of types of supports are referenced from Magics software by Materialize. Accordingly, different types include block support, point support, web support, contour support, and line support.

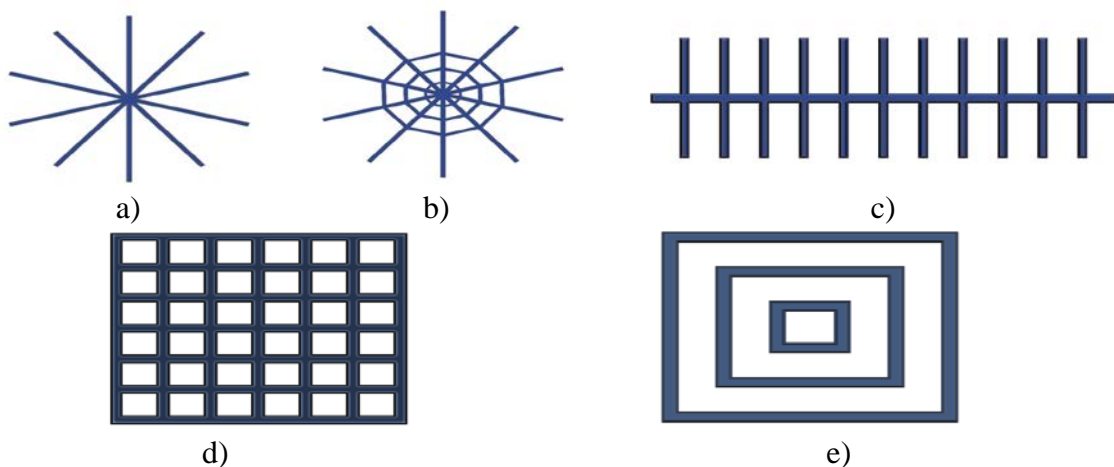


Figure 12. Different types of supports for SLM including a) block support; b) point support, c) web support, d) contour support, and e) line support g [147]

Since the number of possibilities for support types is endless, the design is not just restricted to the traditional geometric structures, now a day bio-mimics are being implemented in this domain. Bio-mimics is the concept where inspiration from existing designs from nature are taken and implemented considering the engineering applications. Examples such as honeycomb structure (Figure 13 a) and fractal geometric structures (Figure 13 b) are some widely used bio-mimics. Such lattice structures can be generated in CAD software using mathematical equations, or now dedicated software can model lattices for fabrication within the software. Optimized structures can help reduce the overall weight of the supports, and this reduces material utilization, build time, total assets, and provide better qualities like surface finish and support removal.

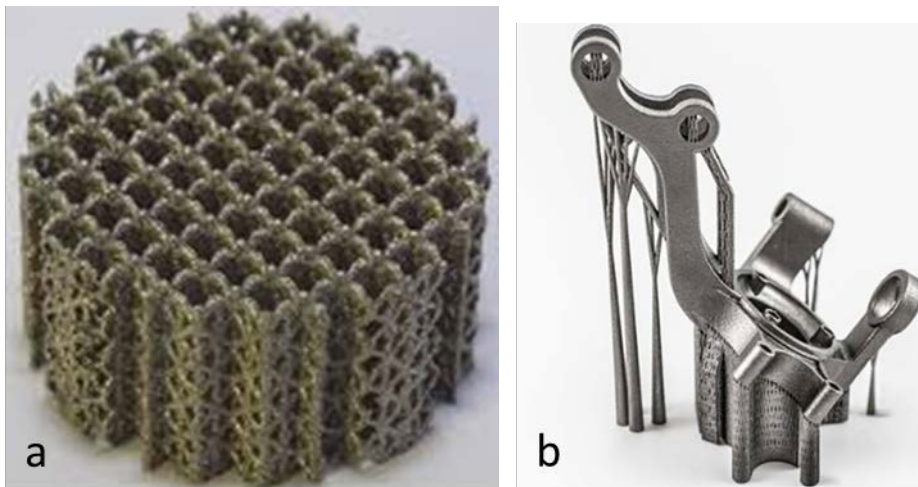


Figure 13. (a) bio-mimics support structures including honeycomb [148]; (b) Fractal used in SLM [149].

### 2.3.6. Metrics of optimizing support structures

A minimum amount of support allocation for the part, to satisfy basic needs that help eliminate the chances of fabrication failure should be considered as an important factor. Restriction on distortion, easy removal, anchor overhanging parts, reduce warping and cracking, etc. should be considered as metrics for an optimized support structure. The recoater continuously spreads the powder during every cycle which can cause defects in thin parts. Supports hold the part to the build plate during every elevation cycle to avoid crashing into a recoater or blade [130].

### 2.3.7. Support Structure optimization

The basic idea behind support optimization is to reduce total fabrication costs by controlling build time, material costs, material wastage, and providing better mechanical and microstructural properties. In general, support optimization is a great design for the AM process and should be applied as much as possible. The following sub-chapters talk more on the process of optimizing support [130].

#### 23.7.1. Optimal orientation

Experimenting with part orientation can be considered as one of the best ways to initiate support optimization. With proper orientation, the printing time, part quality, and surface roughness can have significant enough impact. Different orientation (horizontal, vertical, or angled) requires a different set of supports. Consider a ‘T’ shaped part mentioned as represented in Figure 14a. If the fabrication is initiated for ‘T’ shape, there is a desperate need for supports at the overhanging parts. While if the part is fabricated as ‘L’, the need for supports is eliminated (Figure 14c). Such setup provides an idea of how part orientation affects the fabrication. For a complex part, each side will have different surface topology and hence might require a completely new set of supports for each side. Thus, the fact that the need for supports is dependent on part orientation can be asserted [126, 150].

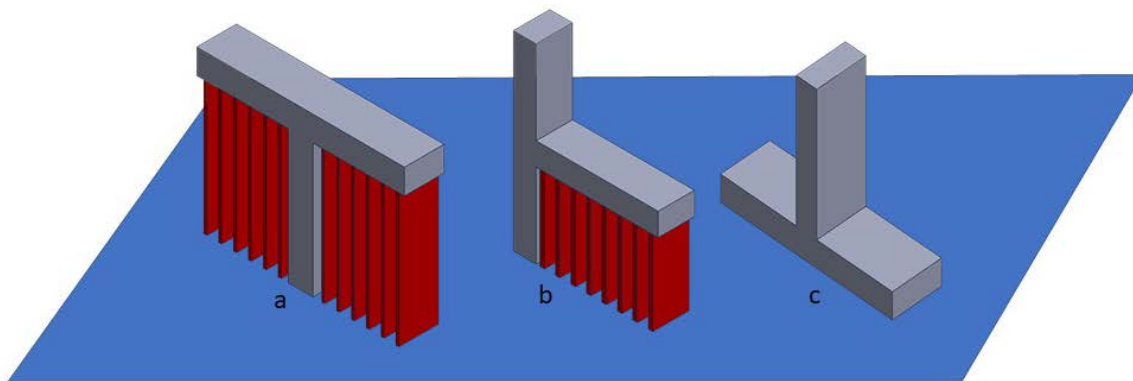


Figure 14. (a) Fabrication of ‘T’ part needing more supports, (b) Orientation shifted by 90° and is requiring lesser supports. (c) Elimination of supports by changing part orientation [126].

### 2.3.7.2. Topology optimization

During circumstances where the supports are an unavoidable entity, topological optimization comes into a picture. Using multiple features like lattice structures can help reduce the total volume and end up saving material, time, and cost. Commonly in 3D printing, the supports allocated are limited to producing vertical structures, which are technically not space-efficient. In such instances, the tree-like support structure can be considered as a viable option (Figure 13b). Studies show these fractal structures reduce the total volume by about 75% when compared to vertical block support of the same dimensions. Software like Autodesk Mesh mixer (California, USA) is oriented towards the creation of such structures for FDM, SLA, and DMLS processes.

### 2.3.7.3. Fillets and chamfers

Having fillets and chamfers for overhangs can reduce the required amount of supports. Since a chamfer is a sloped edge and a fillet is a rounded edge, these features can turn an overhanging surface with an angle of  $45^\circ$  or greater to be less than  $45^\circ$  and can be added to the exterior of the main parts (Figure 15). Material wastage due to excessive supports can be reduced since the need for supports at overhanging surfaces is reduced.

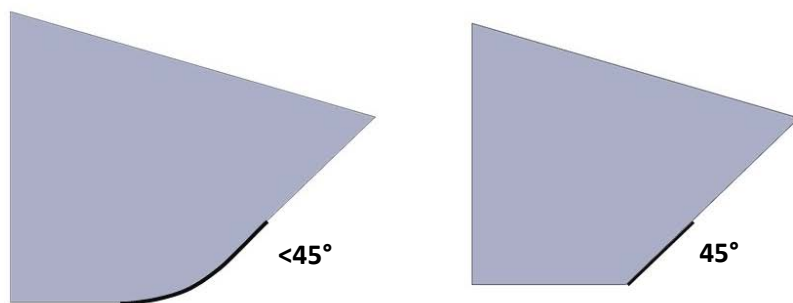


Figure 15. Reduction of critical angle using external features, leading to the elimination of support requirements

#### *2.3.7.4. Splitting main part*

For extremely complex parts, the finish and properties can become slightly undesirable if a lot of supports is allocated. To overcome this challenge, parts can be separately manufactured and then assembled. The main goal behind the process is to speed up the process and save material while reducing support provides subordinate benefits. One issue with this technique is that the assembled part should be in the same build direction to have consistent properties across the main part and reduce the chances of mechanical failure.

#### *2.3.7.5. Support structure volume*

Increasing supports will lead to an increase in build-time and material costs. Material costs take up to 18% of total manufacturing costs in powder-based manufacturing techniques. After machine costs, material costs follow, which provides evidence on the importance of this factor in fabrication setup. With the intentions to reduce the material costs the volume of supports are to be reduced which complements the system with additional benefits such as lesser efforts to remove supports and reduction in post-fabrication costs which takes up to 8% of total fabrication [135] and, adapting to such methods will help in having part properties [151].

#### *2.3.7.6. Support optimization strategy*

At present, topology optimization is still not completely tailored according to the characteristics of AM [152]. For SLM, the inclination of overhanging parts should be above critical value ( $45^\circ$ ) with respect to the baseplate. When this criterion is satisfied, the part can be expressed as self-supporting [153-155].

When the overhangs do not satisfy the criterion, sacrificial supports are supposed to be considered during process design and then removed after processing. But there are several disadvantages associated with such an approach. It should take to the account that modifying optimized geometry will reduce its performance while introducing supports will increase the related costs and time entities.

Several attempts have been conducted to automate the process of support optimization [156-158]. However, the final objective of obtaining the best support structure is the reduction of the support structure by reducing the volume of the structure. In the SLM support optimization approach, first, the settings are arranged, and the main part geometry is imported in a software. The main part geometry is rotated and is set for support generation by using the software. The faces where there is a need for support structure are selected, and appropriate supports are generated. Then the support volume is calculated and is referenced to the previous data. If the update is significant, then the part orientation is investigated. If not, then the process is repeated until the optimal support volume is obtained. Usually, software like magics, Sunata, provide different support structures for various orientation. So, such options can be investigated, and the best one can be selected. The part and the support are exported into an STL file. Sliced model is imported into machine dedicated software like EOSPrint 2, and the fabrication is initiated.

A flowchart that explains the procedure to obtain the best possible support structure is presented in Figure 16.

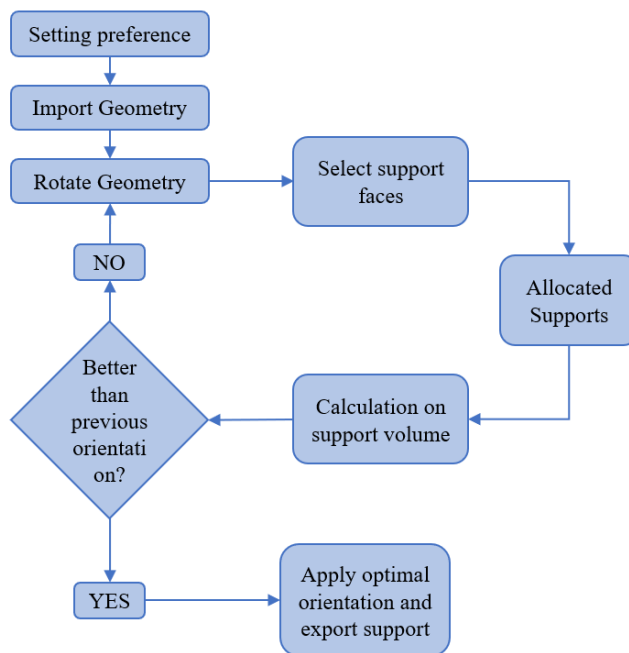


Figure 16. Support generation flowchart explaining step by step procedure for modeling of an optimized support structure [156].

## Chapter 3. Design, fabrication and experimental procedures

### 3.1. CAD design

A total of 15 cubic samples (main part) with a dimension of 8mm x 8mm x 4 mm were modeled using Solidworks 2019 software (version 2018-2019, Dassault Systems, USA). While the main part geometry was simple, the main emphasis was provided to support structures. Here, for each main part, different types of support structure were modeled using Solidworks (version 2018-2019, Dassault Systems, USA) or Magics (V2020, Materialise, Leuven Belgium). Magics is the most common STL editor software using in the AM industry for generating supports. (Figure 17)

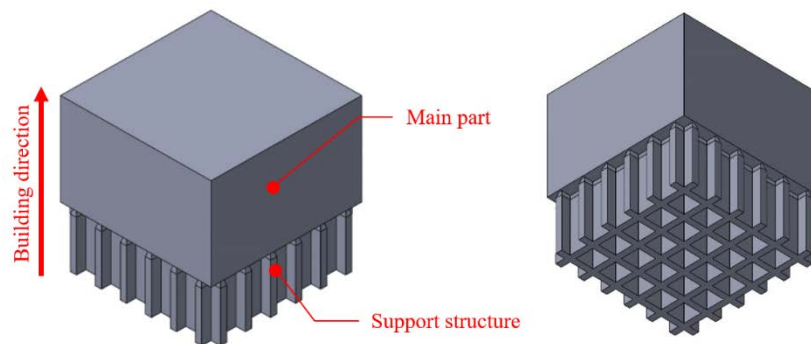


Figure 17. Main fabrication Sample Setup [44].

### 3.2. Support preparation

A total of 4 different types of support structures were modeled in this study. These support structure models are presented in Figure 18. as angled, cone, pin, and concentric types. Apart from the four, a support modelled in Materialize Magics has been introduced in the study.

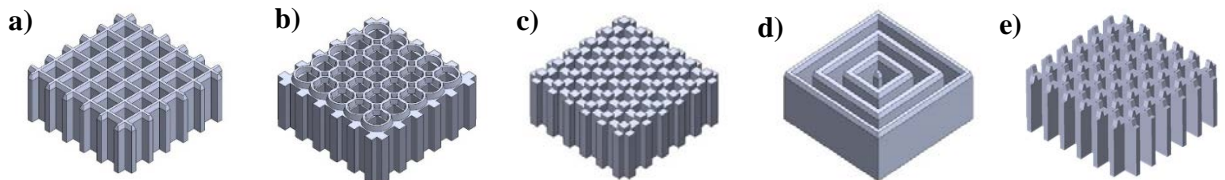


Figure 18. CAD designs of different support structures a) angled; b) cone; c) pin; d) concentric types; e) magics type.

Moreover, different geometrical combinations, including variation in thickness (T) and gap (G) were considered in the design models as it is shown in Figure 19. The basic dimensions for each support structure was 8x8 mm with a constant height of 3 mm in total for all samples. The thickness (T) is the wall thickness of the actual support, and the empty space between two consecutive boundaries of supports is presented as a gap (G). Table 4. summarizes the variation on the type of support structures as well as different geometrical factors (G and T) for each sample.

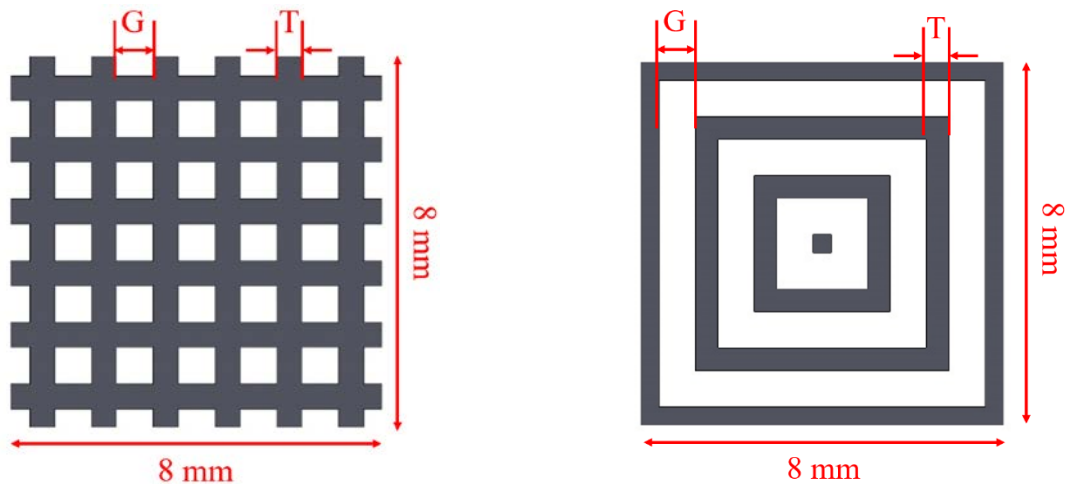
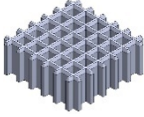
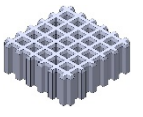
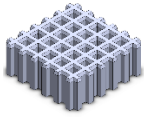
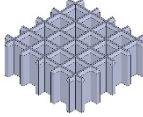
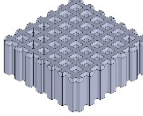
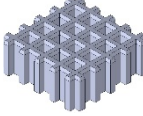
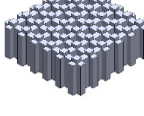
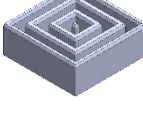
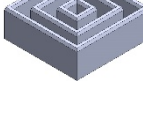
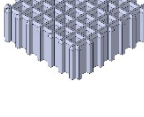
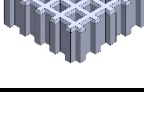


Figure 19. Top view of the grid support structure (left); concentric support structure (right). The thickness of the support wall is presented as “T” and the gap between the neighbor wall is shown as “G”.

Table 4. different types and geometrical factors ( $G$  and  $T$ ) for support structures.

Sample number	Support structure	Thickness (mm)	Gap (mm)	Sample number	Support structure	Thickness (mm)	Gap (mm)
1		0.33	1	9		0.33	0.81
2		0.53	0.8	10		0.33	1.27
3		0.33	1	11		0.53	0.61
4		0.53	0.8	12		0.53	1.07
5		0.53	0.8	13		0.5	0.8
6		0.8	0.8	14		0.45	1
7		0.35	0.8	15		0.33	1
8		0.6	1				

### 3.3 Powder preparation and fabrication

IN718 powder was obtained from EOS Engineering Inc. (Austin, TX). The powder was sieved with a mesh size of 90  $\mu\text{m}$  to avoid inhomogeneity in the distribution of particle size during fabrication.

A DMLS EOS M290 metal 3D printer (EOS GmbH Electro Optical Systems, Germany), equipped with a 400 W Ytterbium fiber laser, was used for the fabrication of all the 15 samples with different support structures. The laser processing parameter set, which was used for fabrication, was recommended by the manufacturer. These laser processing parameters were laser power ( $P$ ) of 285 Watt, scanning speed ( $v$ ) of 960 mm/s, hatch spacing ( $h$ ) of 110  $\mu\text{m}$ , and layer thickness of 40  $\mu\text{m}$ , with an energy density of 67  $\text{J}/\text{mm}^3$  as calculated from equation 2.

$$E = \frac{P}{h \cdot v \cdot t}$$

*Equation 2*



*Figure 20. EOS M290 metal 3D printer with a fiber 400 W laser.*

### **3.4. Sample preparation**

To prepare fabricated samples for experimental procedure, samples were removed from the main part and the build plate using a bandsaw. After support removal, an Allied Techcut 4 precision cutter (Allied

High-Tech, Compton, CA) (Figure 21) was used to cut the main sample 0.8 mm above support through a plane normal to the building direction. The schematic of the cutting strategy is presented in Figure 22.



Figure 21. Allied Techcut 4™ Precision Low Speed Saw used for cutting.

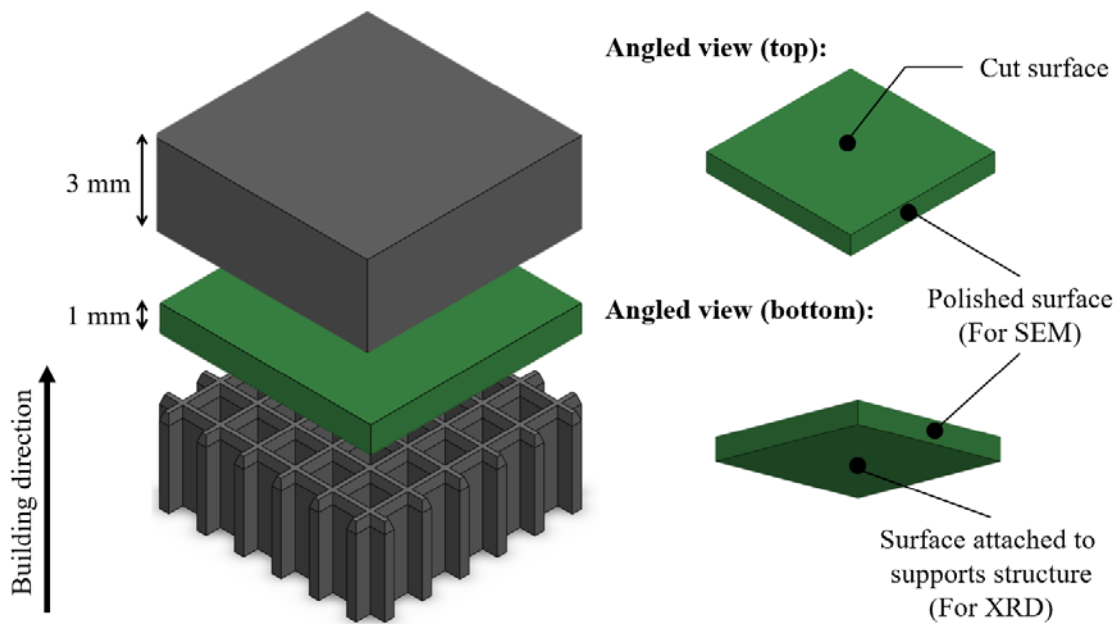


Figure 22. Schematic of separation of the support structure and main part. Also, the cut section of the main part is presented. XRD analysis was conducted on the bottom surface of the main part. The SEM images from the main part were taken from the polished side surface [44].

After this step, the side surface of the cut sample was set in resin and polished using Allied E-PREP 4™ Grinder/Polish machine (Allied High-Tech Products, Inc., Compton, CA) (Figure 23). Here, a standardized polishing strategy was utilized to maintain consistency within the parts being prepared for

SEM investigation. E-prep 4™ polisher was used with polishing sandpaper of grits 180, 320, 600, 800, and 1200, which were used in order to get the initial polished surface with water as a lubricant. Each polishing cycle was done twice for 10 minutes each. After this standard procedure, a ‘DiaMat’ polishing cloth was used with 1 μm polycrystalline diamond suspended solution, and a ‘Red Final C’ polishing cloth was used with 0.5 μm colloidal silica solution. The objective of this procedure was to remove deformations caused by material removal. The time cycle for both ‘DiaMat’ and ‘Red Final C’ polishing cloth was 10 minutes. The machine parts and samples were cleaned with distilled water before every cycle and blown by compressed air to remove any debris.



Figure 23. Allied E-PREP 4™ Grinder/Polish.

### 3.5. Experimental procedures

#### 3.5.1. Scanning electron microscopy (SEM) and Energy Dispersive X-Ray Spectroscopy (EDS)

To evaluate the effect of support structures on the microstructure of the fabricated main parts, a Hitachi S-3000N scanning electron microscope (SEM) was used (Figure 24) at the Characterization Center for Materials and Biology at the University of Texas at Arlington (CCMB-UTA). The device was a PC controlled variable pressure SEM with the ability to switch between the high vacuum and variable pressure modes.

The SEM setup was controlled and monitored by a PC and had the ability to switch between a high vacuum where resolution is 3.0 nm and a low vacuum with 4.0 nm resolution. High-density frame memory of 1280 x 960 pixels was provided by the machine, which was attached to a NORAN 7 integrated EDS/EBSD system.

The machine operated at 20kV in the backscatter electron emission modes. The device was equipped with an energy dispersive X-Ray spectroscopy (EDS) module. The purpose of doing EDS was to determine the elements available on the fresh powder as well as the main parts. SEM imaging was conducted on all 15 main samples near the support zone (on the polished side surface).



*Figure 24. Hitachi S-3000N Scanning Electron Microscope.*

### 3.5.2. X-Ray diffraction (XRD)

Crystal and compositional structures of fresh powder as well as the bottom surface of main fabricated samples (as shown in Figure 22) were determined using Bruker D8 Advance X-ray diffractometer (Figure 25) at CCMB-UTA to determine the compositional of fused metal. The X-ray source was Copper (Cu) k-alpha, and the measurements were conducted at room temperature where the wavelength of X-rays was 1.5406 Å, step intervals of 0.02 and in 2 $\theta$  between 30° and 100° at 1 s/step speed.



*Figure 25. Bruker D8 Advance X- ray diffractometer.*

### 3.5.3. Hardness analysis

The bottom surface of fabricated main parts where attached to the supports (as shown in Figure 22) were used to evaluate the effect of different support types on the Vickers harness of SLM samples. For this objective, a LECO LM 300 Vickers Hardness tester at CCMB-UTA (Figure 26) was used. The test was conducted under 500 g loads applied for 10 seconds. At least three indentations were done to provide a comprehensive report on the average hardness value for each sample.



*Figure 26. LECO LM 300 AT Micro Hardness Tester*

## Chapter 4. Results and discussion

### 4.1. Fabricated samples

Figure 27 shows all the fifteen IN718 samples fabricated with DMLS technique on a stainless-steel substrate. As it is shown, all the identical main parts were fabricated successfully on top of different support structures (i.e., different types such as angled, cone, pin and concentric, or different geometry such as G and T).



*Figure 27. SLM IN718 samples with different support structures fabricated on a stainless-steel building plate.*

### 4.2. Microstructure analysis

An SEM image of fresh powder is presented in Figure 28a. The image revealed that the powder had a spherical shape, acceptable flowability and packing density, low impurity content, and excellent transformation ability. Moreover, the image was used for further analysis of the distribution of particle size using ImageJ software [159]. Figure 28b represents a histogram for the particle-size distributions of fresh IN718 powders. According to the report determined from the analysis of SEM image, an average particle size of 18  $\mu\text{m}$  was found along with nominal particle size distribution ranging from 6 to 30  $\mu\text{m}$ .

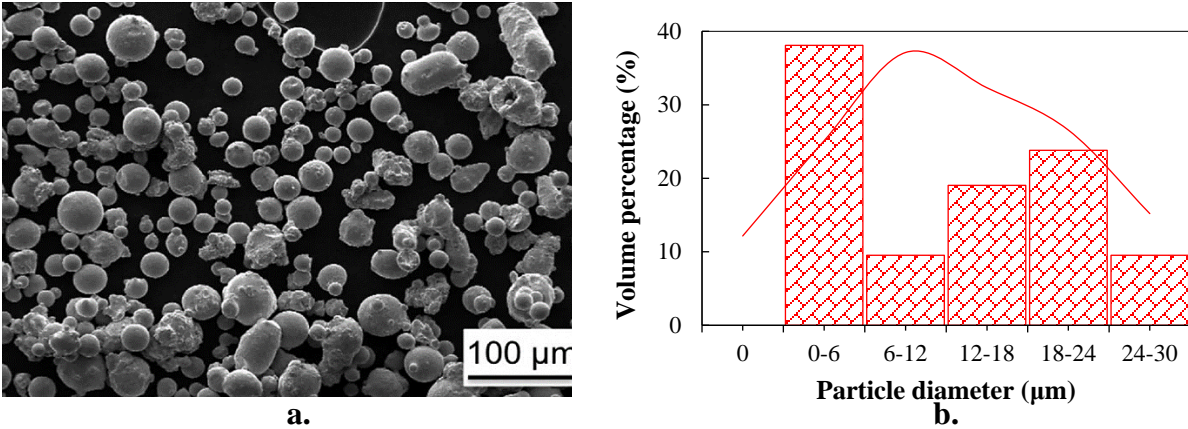
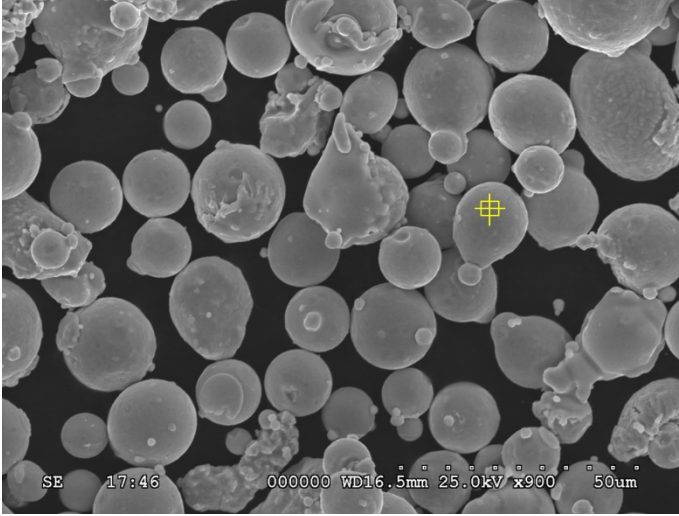


Figure 28. (a) SEM micrograph; (b) particle size distribution for commercial EOS IN 718 powder.

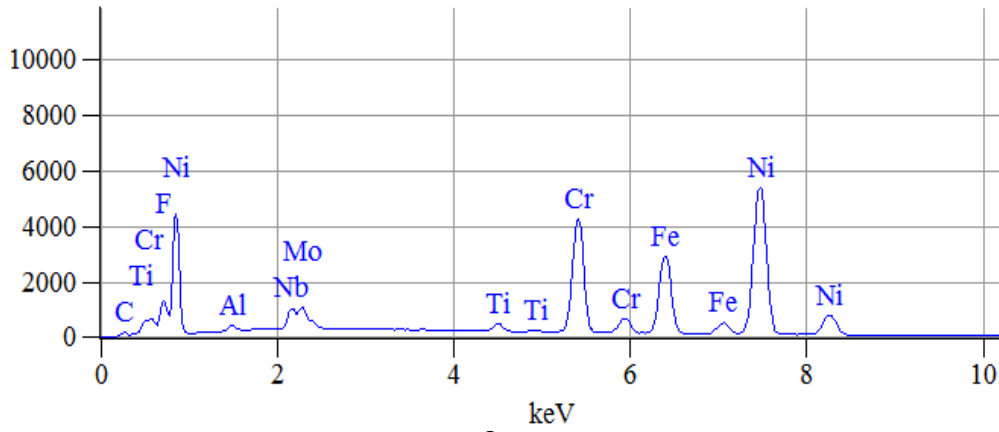
The elemental analysis on the surface of fresh powder particles achieved by EDS is presented in Figure 29. According to the expectations, Ni was the dominant element during analysis, which counted to 52% wt. After comparing the constitution of fresh IN718 powder and wrought IN718 sample, the chromium concentration was higher by 2% in fresh powder analysis. This assists in improving the oxidation resistance of additively manufactured samples [160]. On the other hand, iron content in fresh powder was 1% more than wrought samples, which can cause negative impacts.



Wt. %	C
C	1.33
F	1.00
Al	0.36
Ti	1.19
Cr	20.03
Fe	17.76
Ni	52.22
Nb	3.64
Mo	2.47

a.

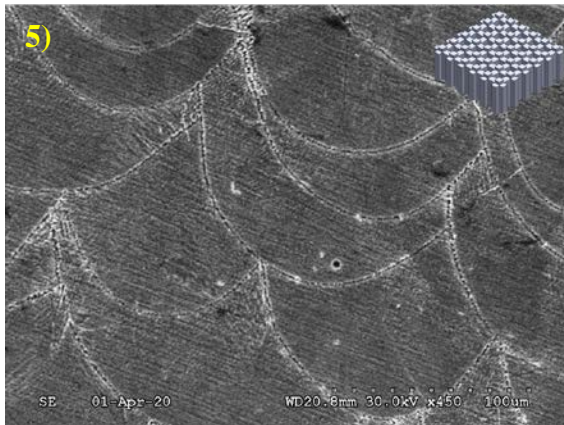
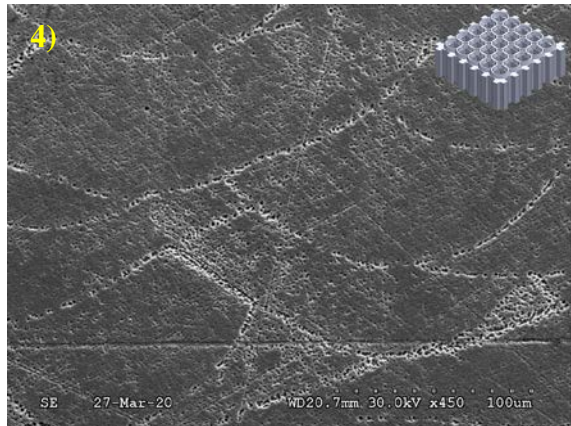
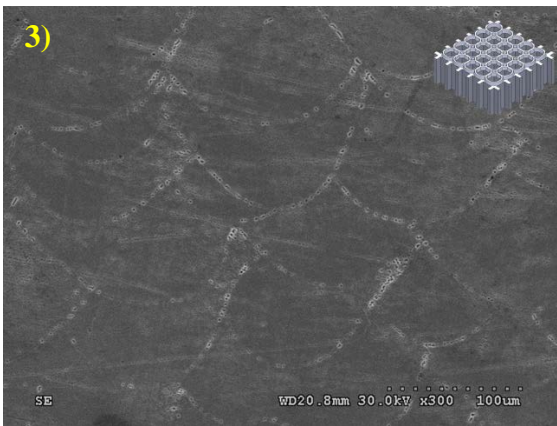
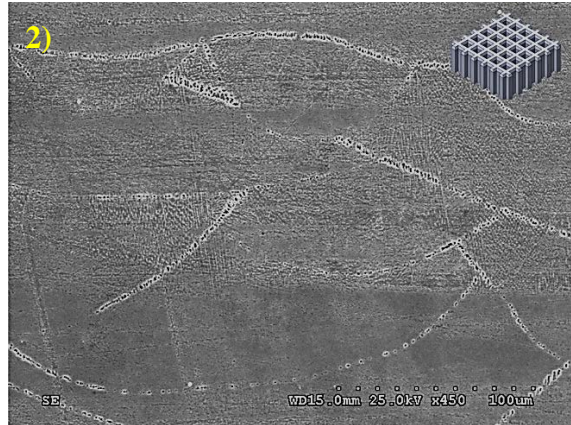
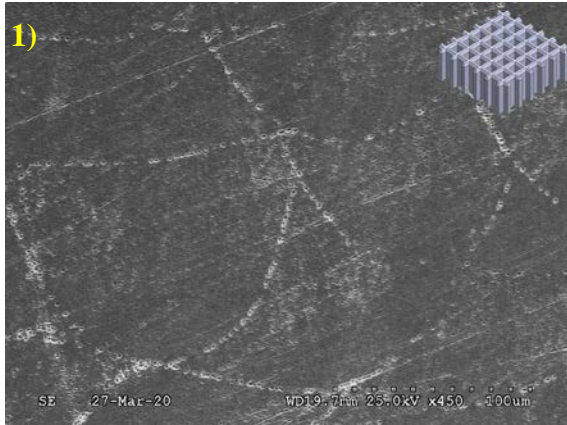
b.

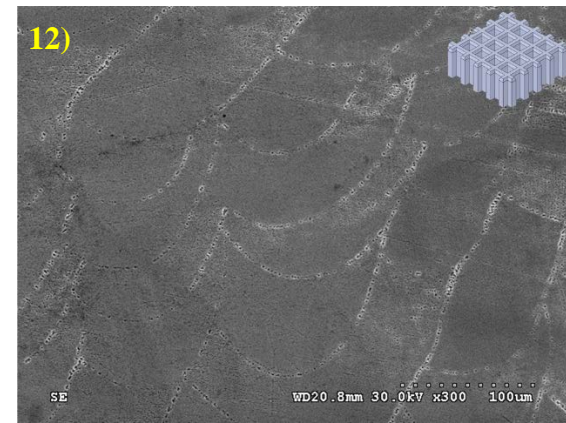
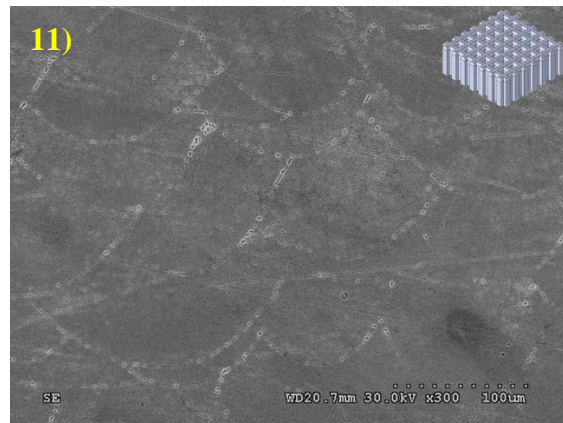
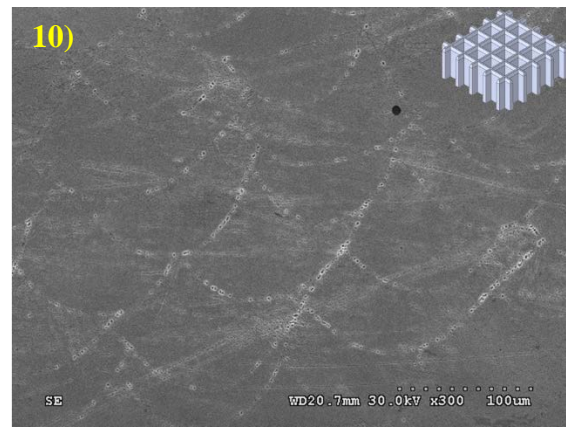
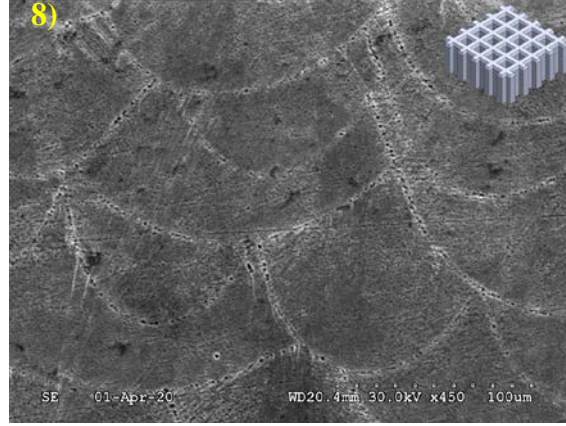
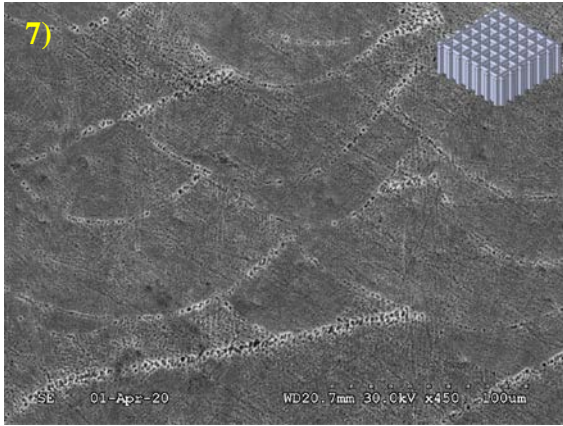


c.

Figure 29. (a) SEM of fresh IN718 powder; (b) table describing percentage composition for each element; (c) EDS compositions of IN718 fresh powder tested.

Then the SEM image of the side surface (as it's shown in Figure 22) of main parts along the building direction is presented in Figure 30. The images reveal melt pools with a Gaussian shape due to the laser beam passes of each layer. As it is clear, different support structures have effect on the melt pool size and shape in the side surface of fabricated parts near the support structure. The average melt pool depth varies from 35  $\mu\text{m}$  (for sample #4) to 65  $\mu\text{m}$  (for sample #8). With an increase in the melt pool depth, a better columnar grain structure was achieved. From Figure 30 we can see that the columnar structure growth is parallel to the laser direction.





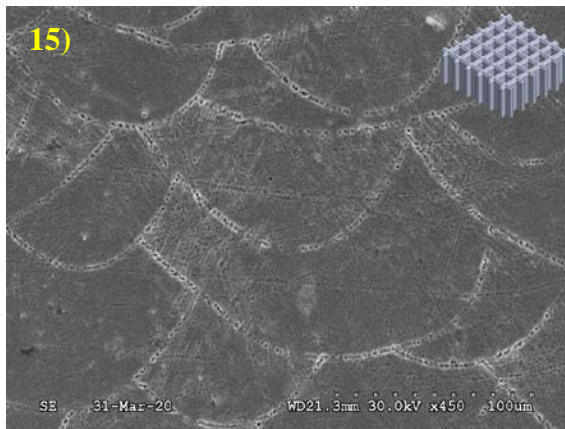
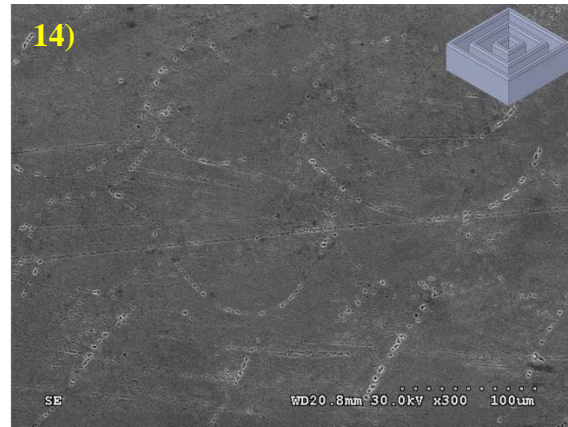
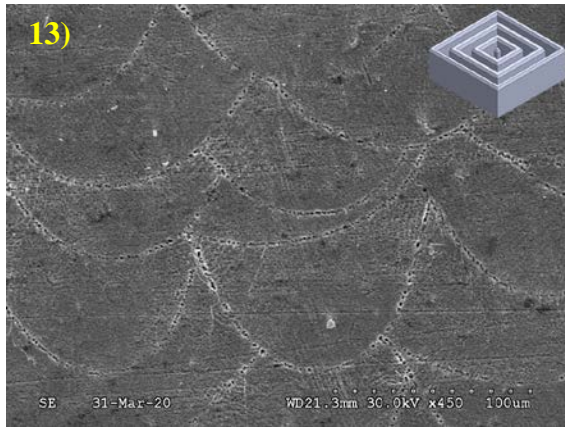
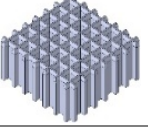
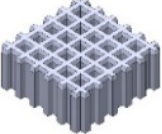
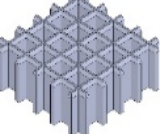
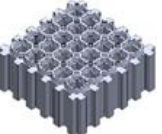
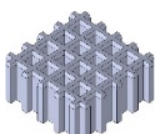
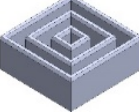
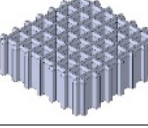
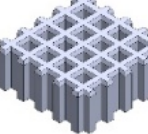


Figure 30. SEM images of melt pool size for 1) angled (thickness=0.33; gap=1); 2) angled (thickness=0.53 ; gap=0.8); 3) cone (thickness=0.33; gap=1); 4) cone (thickness=0.53; gap=0.8); 5) pin (thickness= 0.53 ; gap=0.8); 6) T variation (thickness= 0.8; gap=0.8); 7) T variation (thickness=0.35; gap=0.8); 8) T variation (thickness=0.6; gap=1); 9) G Variation (thickness=0.33; gap=0.81); 10) G Variation (thickness=0.33; gap=1.27); 11) G Variation (thickness=0.53; gap=0.61); 12) G Variation (thickness=0.53; gap=1.07); 13) Concentric ( thickness=0.5; gap=0.8) 14) Concentric (thickness=0.45; gap=1) 15) Magics (thickness= 0.33 ; gap=1).

Grain aspect ratio is the term used to determine the grain structure. There are two methods to find aspect ratios; by EBSD and other by aspect ratio formula. The formula for aspect ratio is the ratio of minor axis (a vertical measurement of grain size) to the major axis (a horizontal measurement of grain size). The value of the aspect ratio ranges from 0 to 1. When the values are between 0 to 0.3, the grain growth is columnar. While if the ratio is more than 0.3, the growth is equiaxed, and if the values are between 0.3 to 0.4, the grain structure is called Columnar to Equiaxed Transition (CET) [161]. The grain structure of sample 4, 5 and 15 is cellular, sample 7 and 8 is columnar and for sample 13 is equiaxial.

Table 5. Effect of support structures on the melt pool size and grain structure on the side of the fabricated part near the support zone.

Sample	Support Structure	Average		Sample	Support Structure	Average	
		Depth ( $\mu\text{m}$ )	Width ( $\mu\text{m}$ )			Depth ( $\mu\text{m}$ )	Width ( $\mu\text{m}$ )
Sample #1		60	147	Sample #9		65	191
Sample #2		47	143	Sample #10		61	132
Sample #3		44	145	Sample #11		63	114
Sample #4		35	156	Sample #12		49	135
Sample #5		36	125	Sample #13		63	156
Sample #6		54	135	Sample #14		41	126
Sample #7		50	126	Sample #15		44	129
Sample #8		65	106				

From Table 5, an idea on the average depth of melt pool can be acquired. The melt pool depth ranges from 35  $\mu\text{m}$  to 65  $\mu\text{m}$ , while the layer thickness is just 40  $\mu\text{m}$ . Sample 13 which is concentric in

type, provides the maximum depth while the maximum width is for sample 4 (cone) and sample 13 (concentric). As it was observed, the sample 13 provides the biggest melt pools.

### 4.3. Compositional Analysis

Compositional analysis was performed using XRD on the plate facing support structures (as discussed in Figure 22) for each SLM fabricated IN718 sample, and results are presented in Figure 31. As it was expected, different phases for the fresh powder and all 15 SLM IN718 samples were found to be  $\gamma$  (Ni, Cr, Fe, C),  $\gamma'$  (Ni<sub>3</sub>(Al,Ti)),  $\gamma''$  (Ni<sub>3</sub>Nb) and  $\delta$  (C(Ni,Ti)). As shown, XRD peaks occur at the almost same angle in each fabricated sample (at  $2\theta$  equal to 44°, 51°, 75°, and 90°, respectively).

The interpretation of XRD results reveals that the support structure has a direct effect on the composition of the main part. The  $\gamma$ ,  $\gamma'$  and  $\gamma''$  phases for fresh powder, and each specimen are presented in Table 6. As it was expected  $\gamma$  phase found to be the major phase in all of the fabricated samples (45.8-81%), and the rest comprised mostly of  $\gamma'$  and  $\gamma''$  phases.  $\delta$  phase was also presented in traces and had properties similar to that of  $\gamma''$  phase. While there are traces of  $\delta$  phase in the supports, the quantity when compared to  $\gamma$ ,  $\gamma'$  and  $\gamma''$  phases are extremely negligible and hence can be neglected. In comparison, the  $\gamma''$  in sample was higher than other samples. This phase ( $\gamma''$  (Ni<sub>3</sub>Nb precipitate)) is associated with higher strength of fabricated part up to 650 °C [162].

With increase in the strengthening phase, there is an increase in hardness of the samples. The main strengthening phase is the  $\gamma'$  phase. With increase in temperature, the  $\gamma'$  evolves to  $\gamma''$  which with more increase in temperature leads conversion of  $\gamma''$  to  $\delta$  phase. The  $\delta$  phase is a brittle, due to which, the quantity of  $\delta$  phase should be less within the system. Phase composition of sample 2 contains most strengthening phase followed by 4.

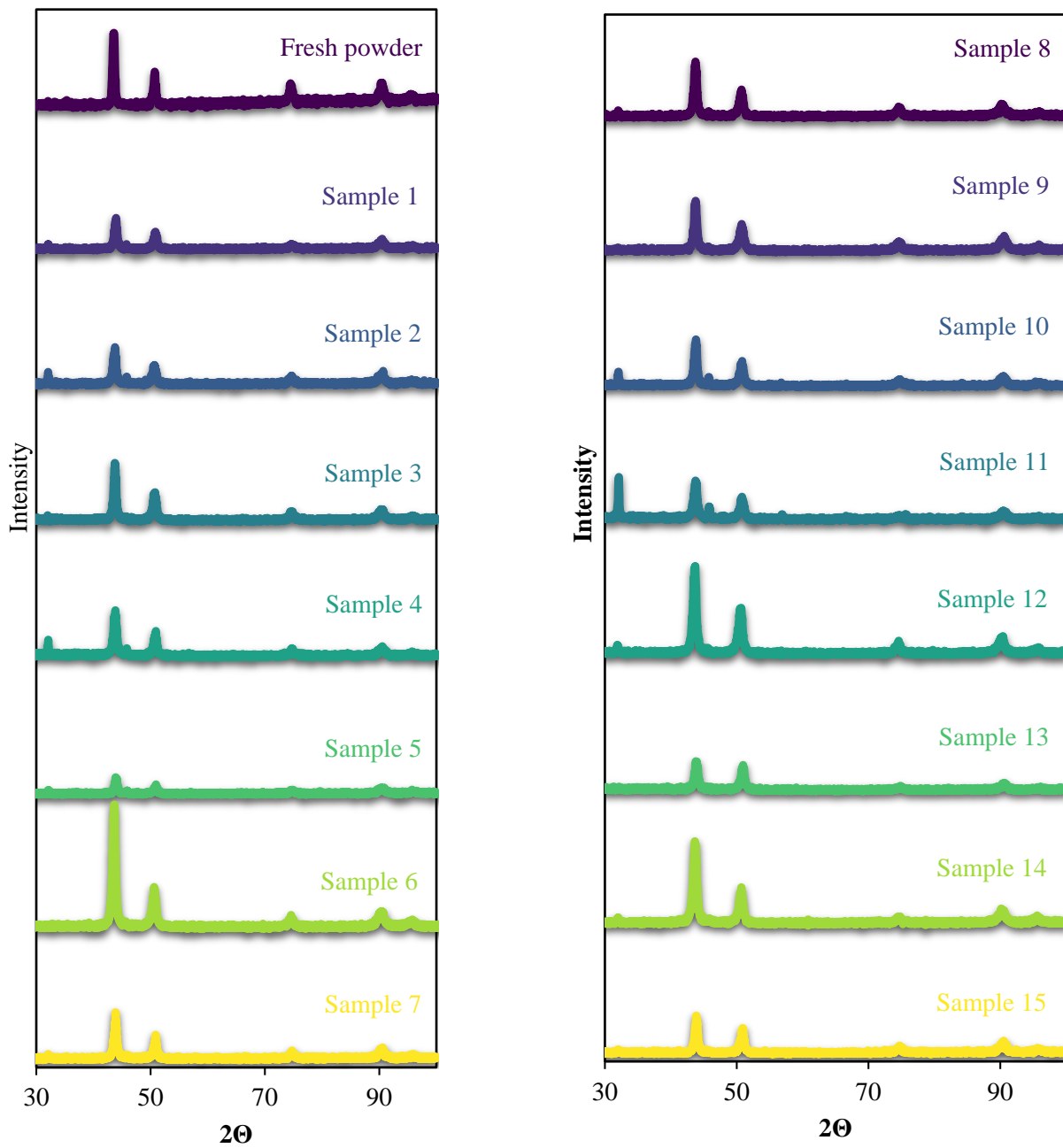


Figure 31. XRD image of fresh powder and 15 samples.

Table 6. Calculation of % area of phases for the fabricated IN718 sample on top of different support structures (With the intention of eliminating noise in the system, a minimum intensity value is kept for all graphs. Peaks with values more than the minimum intensity are detected, and the areas are represented.)

Support structure	Peak	Y Area%	Y Area%	Y Area%
<b>Fresh powder</b>	1	70.61	29.39	0
	2	74.45	19.64	5.89
	3	100	0	0
<b>Sample #1</b>	1	74.2	25.7	0
	2	55.1	34.9	9.9
	3	62.8	22.0	15.1
<b>Sample #2</b>	1	72.73	27.26	0
	2	54.22	33.08	12.69
	3	55	44.99	0
	4	54.36	32.23	13.39
<b>Sample #3</b>	1	76.29	23.7	0
	2	64.87	20.955	14.16
	3	64.63	35.369	0
	4	60.79	24.12	15.08
<b>Sample #4</b>	1	56.9	43.0	0
	2	66.7	20.6	12.6
	3	81.3	18.7	0
	4	58.3	23.5	18.1
<b>Sample #5</b>	1	72.7	27.2	0
	2	51.6	42.1	6.2
<b>Sample #6</b>	1	73.37	23.63	0
	2	51.60	39.45	8.93
	3	72.19	23.91	0
	4	58.7	22.67	18.63
<b>Sample #7</b>	1	54.6	45.3	0
	2	67.9	16.3	15.7

	3	73.7	26.2	0
	4	57.9	25.9	16.1
<b>Sample #8</b>	1	68.4	31.1	0
	2	61.7	26.4	11.8
	3	66.1	33.9	0
	4	63.5	20.4	16.1
<b>Sample #9</b>	1	56.42	43.58	0
	2	64.48	20.26	15.24
	3	73.59	26.4	0
<b>Sample #10</b>	1	78.82	21.28	0
	2	0	0	100
	3	85.88	12.37	1.74
<b>Sample #11</b>	1	72.54	27.45	0
	2	0	100	0
	3	80.94	5.02	5.12
<b>Sample #12</b>	1	75.96	24.06	0
	2	68.97	18.60	12.42
	3	58.30	22.76	18.94
	4	55.83	44.16	0
<b>Sample #13</b>	1	50.0	49.9	0
	2	65.1	23.6	11.1
	3	45.8	45.7	8.3
<b>Sample #14</b>	1	76.55	23.44	0
	2	64.94	19.01	16.313
	3	100	0	0
<b>Sample #15</b>	1	68.1	31.9	0
	2	66.5	17.4	15.9
	3	78.1	21.9	0

#### **4.4. Hardness analysis**

Vickers Hardness values were measured on the bottom surface of the main parts for all the 20 samples, as presented in Table 7. To eliminate the chances of errors, 3 trials of indentations were conducted. And consequently, 3 hardness values were calculated through which an average hardness value was used for further comparison of hardness properties of the supports. It is seen that the angled type support has an effect on the hardness of the main part. After calculating the hardness values for all 15 samples, it can be observed that the maximum hardness value was for sample 9, which is the angled type sample. From Table 7, it can be interpreted that the maximum hardness value of 460.5 Hv corresponds to sample 5 and the least to sample 15. With an increase in thickness, the hardness value of the samples increases.

Table 7. Hardness values on the bottom side of all main parts facing support structures

Support structure	Measured L <sub>1</sub> and L <sub>2</sub>			Hardness			average
	1 <sup>st</sup> trial	2 <sup>nd</sup> trial	3 <sup>rd</sup> trial	1 <sup>st</sup> trial	2 <sup>nd</sup> trial	3 <sup>rd</sup> trial	
Sample 1	50.1	50.6	48.7	363.6	360.5	386.0	370.0
	50.9	50.9	49.3				
Sample 2	50.1	55.1	50.2	375.9	288.1	360.8	341.6
	49.3	58.4	51.1				
Sample 3	38.3	48.1	49.1	516.8	391.4	425.2	444.5
	46.4	49.3	44.3				
Sample 4	48.0	46.3	42.7	368.4	357.4	338.2	354.6
	52.4	55.5	62.1				
Sample 5	58.2	38.3	45.2	284.0	652.5	445.0	460.5
	56.0	37.1	46.1				
Sample 6	53.1	50.5	48.6	348.6	368.2	364.6	360.5
	50.1	49.9	52.3				
Sample 7	47.5	47.7	50.5	390.8	398.9	368.2	386.0
	49.9	48.7	49.9				
Sample 8	53.1	50.9	51.6	348.6	373.3	367.4	363.1
	50.1	48.7	48.9				
Sample 9	43.1	48.6	49.6	672.4	364.6	368.1	468.3
	31.2	52.3	50.8				
Sample 10	49.3	47.7	56.6	375.4	397.7	334.9	369.3
	50.1	48.9	48.6				
Sample 11	51.8	44.7	53.0	398.7	471.2	356.5	408.8
	44.7	44.1	49.0				
Sample 12	48.8	56.6	49.4	389.7	334.9	379.4	368.0
	48.7	48.6	49.5				
Sample 13	49.3	50.7	54.3	375.4	385.3	315.4	358.7
	50.1	47.4	54.2				
Sample 14	49.6	47.7	51.3	425.1	397.7	377.5	400.1
	43.8	48.9	47.8				
Sample 15	67.3	49.8	62.6	280.7	427.9	275.1	327.9
	47.6	43.3	53.6				

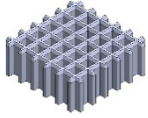
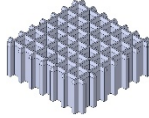
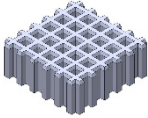
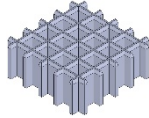
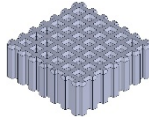
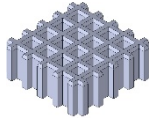
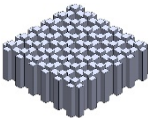
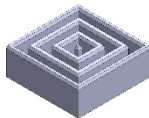
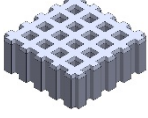
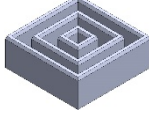
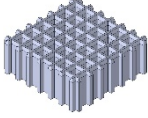
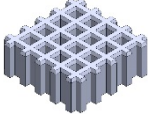
#### **4.5. Build time and material cost estimation**

In AM, the freedom of manufacturing a complex part provides a massive advantage over conventional manufacturing techniques. While the advantages are immense, the direct costs (machine cost, build time, material cost, etc.) incurred during fabrication should be reduced as much as possible, to obtain better and profitable outputs. By successful implementation of this strategy AM can have a better adaptation in the industry. As the build time increases, the cost of running for resources that help run the fabrication system also increases, and the same goes for material costs. Thus, while optimizing a design or deciding a better support alternative, the material cost and build time should be minimum. Since the material required is directly dependent on the volume of the support, the least support volume is preferred.

From Table 8, sample 3 has the least support volume. Since the support height for all the samples is the same, the build time is consistent for all manufactured parts, i.e., 12.23 minutes. Thus, for cost-wise estimation, since there is consistent build time, the decision can be taken based on the least amount of support volume, i.e., sample number 3 has the minimum build time.

It can be interpreted that the best choice considering build time and material costs is sample 3.

Table 8. Calculation for build time and support volume for all supports geometries.

Sample	Support structure	Building time	Support volume	Sample	Support structure	Building time	Support Volume
Sample 1		12.23	81.1	Sample 9		12.23	92.43
Sample 2		12.23	120.46	Sample 10		12.23	69.14
Sample 3		12.23	80.27	Sample 11		12.23	134.81
Sample 4		12.23	115.49	Sample 12		12.23	104.46
Sample 5		12.23	113.11	Sample 13		12.23	80.87
Sample 6		12.23	142.63	Sample 14		12.23	73.79
Sample 7		12.23	97.2	Sample 15		12.23	79
Sample 8		12.23	115.41				

## Chapter 5. Conclusions and Future Works

### 5.1. Conclusion

It was revealed that the powder had a spherical shape, acceptable flowability and packing density, low impurity content, and excellent transformation ability. The average melt pool depth varied from 35  $\mu\text{m}$  to 65  $\mu\text{m}$ , with the highest value for the Angled-type having the thickness of 1 mm and gap of 0.6 mm. With an increase in the melt pool depth, a better columnar grain structure was achieved.

It was found that an increase in hardness values is the consequence of relatively higher degree of the  $\gamma'$ . From Table 6 and Table 7, the amount of  $\gamma'$  precipitate in sample 5 (pin type) is relatively high (32.65% of the entire constituent phases), which is a reason for greater hardness value of 460.5 Hv. To compare the relation for this factor, sample 15 (magics type) with the low hardness value of 352.9 Hv, has the  $\gamma'$  precipitate of 26.21%, which again is low, thus provides us a reference on the direct relationship of the hardness value and the strength hardening precipitate. The hardness values of sample 9 and 5 are close to each other with sample 9 having a slightly higher value. After comparing the  $\gamma'$  composition percentage, the values are close to each other (32%) but the  $\gamma''$  for sample 9 is more than for sample 5. The  $\gamma''$  composition percentage for sample 9 is 6.74% and the value for sample 5 is 2.56%, which provides a valid explanation for hardness value of sample 9 being greater than sample 5 since  $\gamma''$  is another strengthening phase.

A relationship between support thickness and the hardness was observed from the interpreted results. With the increase in thickness for the support, the amount of area in contact with the main part increases. Thus, the increased contact area leads to increasing heat transfer from the sample to the substrate which can cause a reduction in the amount of energy within the sample. This reduction may not provide enough energy to have  $\gamma'$  and  $\gamma''$  precipitate in the fabricated IN718 samples and decreases the strength hardening phase in the main sample and thus lesser hardness values. Accordingly, with lower hardness values, shallower melt pools were observed. Thus the contact area between the supports and the main part is important and has a direct effect on the hardness property of the samples.

The cost of production is dependent on the volume of support that is allocated, since it affects the direct costs of fabrication, material, along with other factored. After comparing the samples, the maximum support volume is for sample 6 and the minimum is for sample 15 (Table 8). Thus sample 15 provides the results at the minimum cost with a hardness value of 352.9 Hv which lies in the optimal range for IN718. Also, the grain structure is cellular, which imparts favorable hardness characteristics. Thus, considering the hardness values, melt pool depth and the cost estimation, we can determine sample 15 will provide the best output for the value.

## **5.2. Future Work**

For AM parts, the grain structure changes from the support side towards the top, along the build direction, thus investigation for changes in microstructure can be obtained. Since AM deals with multiple parameters such as hatch spacing, scanning strategy, laser speed, laser power, etc. variation in these process parameters can change the properties of the supports and hence main parts. Therefore, a study can be performed to establish the relationship between the process parameters and the final properties of the main parts, particularly near the substrate. Other study can be the influence of supports structures on the IN718 phases along the build direction. Also, the same study can be conducted for more complex structures which can consist of lattice structures or bio-mimics supports.

## Reference

1. Elahinia, M., et al., Fabrication of NiTi through additive manufacturing: A review. *Progress in Materials Science*, 2016. 83: p. 630-663.
2. Moghaddam, N.S., et al., Anisotropic tensile and actuation properties of NiTi fabricated with selective laser melting. *Materials Science and Engineering: A*, 2018. 724: p. 220-230.
3. Farhang, B., et al., Study on variations of microstructure and metallurgical properties in various heat-affected zones of SLM fabricated Nickel–Titanium alloy. *Materials Science and Engineering: A*, 2020: p. 138919.
4. Moghaddam, N.S., et al., Recent advances in laser-based additive manufacturing, in *Laser-Based Additive Manufacturing of Metal Parts*. 2017, CRC Press. p. 1-24.
5. Berdine, G.G., M. DiPaola, and M. Weinberg, Economic and Regulatory Perspectives on Additive Manufacturing, in *3D Printing in Orthopaedic Surgery*. 2019, Elsevier. p. 41-48.
6. Andani, M.T., et al., Metals for bone implants. Part 1. Powder metallurgy and implant rendering. *Acta biomaterialia*, 2014. 10(10): p. 4058-4070.
7. Baufeld, B., E. Brandl, and O. Van der Biest, Wire based additive layer manufacturing: Comparison of microstructure and mechanical properties of Ti–6Al–4V components fabricated by laser-beam deposition and shaped metal deposition. *Journal of Materials Processing Technology*, 2011. 211(6): p. 1146-1158.
8. Gibson, I., D.W. Rosen, and B. Stucker, Sheet lamination processes, in *Additive Manufacturing Technologies*. 2010, Springer. p. 223-252.
9. Lou, A. and C. Grosvenor, Selective laser sintering, birth of an industry. Department of Mechanical Engineering, University of Texas, Austin, TX, 2012.
10. Kabir, S.F., K. Mathur, and A.-F.M. Seyam, A critical review on 3D printed continuous fiber-reinforced composites: History, mechanism, materials and properties. *Composite Structures*, 2020. 232: p. 111476.
11. Deckard, C.R., Method and apparatus for producing parts by selective sintering. 1989, Google Patents.
12. EOS GmbH. History. April 16; Available from: <https://www.eos.info/30-years-of-EOS>.
13. Harun, W., et al., A review of powdered additive manufacturing techniques for Ti-6Al-4V biomedical applications. *Powder Technology*, 2018. 331: p. 74-97.
14. EBM, P., LENS, and Polyjet were nonexistent Arcam-AB,, Arcam History. April 16.
15. Wohlers, T. and T. Gornet, History of additive manufacturing. *Wohlers report*, 2014. 24(2014): p. 118.
16. Kruth, J.-P., Material in-process manufacturing by rapid prototyping techniques. *CIRP annals*, 1991. 40(2): p. 603-614.
17. Bourell, D.L., *Rapid prototyping journal*. 2007, EMERALD GROUP PUBLISHING LIMITED 60/62 TOLLER LANE, BRADFORD BD8 9BY, W ....
18. Sells, E., et al., RepRap: the replicating rapid prototyper: maximizing customizability by breeding the means of production, in *Handbook of Research in Mass Customization and Personalization: (In 2 Volumes)*. 2010, World Scientific. p. 568-580.
19. Es-Said, O., et al., Effect of layer orientation on mechanical properties of rapid prototyped samples. *Materials and Manufacturing Processes*, 2000. 15(1): p. 107-122.
20. Gardan, J., Additive manufacturing technologies: state of the art and trends. *International Journal of Production Research*, 2016. 54(10): p. 3118-3132.
21. Wong, K.V. and A. Hernandez, A review of additive manufacturing. *International scholarly research notices*, 2012. 2012.
22. Jia, Q. and D. Gu, Selective laser melting additive manufactured Inconel 718 superalloy parts: high-temperature oxidation property and its mechanisms. *Optics & Laser Technology*, 2014. 62: p. 161-171.

23. Raghavan, N., et al., Numerical modeling of heat-transfer and the influence of process parameters on tailoring the grain morphology of IN718 in electron beam additive manufacturing. *Acta Materialia*, 2016. 112: p. 303-314.
24. Tillmann, W., et al., Hot isostatic pressing of IN718 components manufactured by selective laser melting. *Additive Manufacturing*, 2017. 13: p. 93-102.
25. Körner, C., et al. Tailoring the grain structure of IN718 during selective electron beam melting. in *MATEC Web of Conferences*. 2014. EDP Sciences.
26. Hinojos, A., et al., Joining of Inconel 718 and 316 Stainless Steel using electron beam melting additive manufacturing technology. *Materials & Design*, 2016. 94: p. 17-27.
27. Lambert, D.M., IN718 additive manufacturing properties and influences. 2015.
28. Zhang, Y., X. Cao, and P. Wanjara, Microstructure and hardness of fiber laser deposited Inconel 718 using filler wire. *The International Journal of Advanced Manufacturing Technology*, 2013. 69(9-12): p. 2569-2581.
29. Popovich, V., et al., Functionally graded Inconel 718 processed by additive manufacturing: Crystallographic texture, anisotropy of microstructure and mechanical properties. *Materials & Design*, 2017. 114: p. 441-449.
30. Tian, Y., et al., Rationalization of microstructure heterogeneity in INCONEL 718 builds made by the direct laser additive manufacturing process. *Metallurgical and Materials Transactions A*, 2014. 45(10): p. 4470-4483.
31. Moussaoui, K., et al., Effects of Selective Laser Melting additive manufacturing parameters of Inconel 718 on porosity, microstructure and mechanical properties. *Materials Science and Engineering: A*, 2018. 735: p. 182-190.
32. Gangireddy, S., et al., Microstructure and mechanical behavior of an additive manufactured (AM) WE43-Mg alloy. *Additive Manufacturing*, 2019. 26: p. 53-64.
33. Yadroitsev, I. and I. Smurov, Selective laser melting technology: from the single laser melted track stability to 3D parts of complex shape. *Physics Procedia*, 2010. 5: p. 551-560.
34. Huang, S., et al., Influence of surface on spectroscopic properties of rare earth ions in nanocrystals. *Journal of Rare Earth*, 2007. 25(4): p. 396-401.
35. Elahinia, M., et al. Site-specific material properties and the additive manufacturing of nitinol musculoskeletal implants. in *Tissue Engineering Part A*. 2014. MARY ANN LIEBERT, INC 140 HUGUENOT STREET, 3RD FL, NEW ROCHELLE, NY 10801 USA.
36. Amerinatanzi, A., et al., Application of the superelastic NiTi spring in ankle foot orthosis (AFO) to create normal ankle joint behavior. *Bioengineering*, 2017. 4(4): p. 95.
37. Shayesteh Moghaddam, N., et al., Fixation release and the bone bandaid: A new bone fixation device paradigm. *Bioengineering*, 2017. 4(1): p. 5.
38. Zhang, B., H. Liao, and C. Coddet, Microstructure evolution and density behavior of CP Ti parts elaborated by self-developed vacuum selective laser melting system. *Applied surface science*, 2013. 279: p. 310-316.
39. Dong, L. and H. Wang, Microstructure and corrosion properties of laser-melted deposited Ti<sub>2</sub>Ni<sub>3</sub>Si/NiTi intermetallic alloy. *Journal of Alloys and Compounds*, 2008. 465(1-2): p. 83-89.
40. Zhang, B., H. Liao, and C. Coddet, Selective laser melting commercially pure Ti under vacuum. *Vacuum*, 2013. 95: p. 25-29.
41. Saedi, S., et al., Shape memory response of porous NiTi shape memory alloys fabricated by selective laser melting. *Journal of Materials Science: Materials in Medicine*, 2018. 29(4): p. 40.
42. Ahmadi, A., et al. Finite element modeling of selective laser melting 316l stainless steel parts for evaluating the mechanical properties. in *International Manufacturing Science and Engineering Conference*. 2016. American Society of Mechanical Engineers.
43. Moghaddam, N.S., et al. The effect of adding dental implants to the reconstructed mandible comparing the effect of using Ti-6Al-4V and NiTi hardware. in *Tissue Engineering Part A*. 2015. MARY ANN LIEBERT, INC 140 HUGUENOT STREET, 3RD FL, NEW ROCHELLE, NY 10801 USA.

44. Thakare, S., et al. The effect of support structure geometry on surface topography of selectively laser melted parts. in *Behavior and Mechanics of Multifunctional Materials IX*. 2020. International Society for Optics and Photonics.
45. Frazier, W.E., Metal additive manufacturing: a review. *Journal of Materials Engineering and Performance*, 2014. 23(6): p. 1917-1928.
46. Jia, Q. and D. Gu, Selective laser melting additive manufacturing of Inconel 718 superalloy parts: Densification, microstructure and properties. *Journal of Alloys and Compounds*, 2014. 585: p. 713-721.
47. Shahzad, K., et al., Additive manufacturing of zirconia parts by indirect selective laser sintering. *Journal of the European Ceramic Society*, 2014. 34(1): p. 81-89.
48. Chua, C.K., K.F. Leong, and C.S. Lim, *Rapid prototyping: principles and applications (with companion CD-ROM)*. 2010: World Scientific Publishing Company.
49. Kruth, J.-P., et al., Consolidation phenomena in laser and powder-bed based layered manufacturing. *CIRP annals*, 2007. 56(2): p. 730-759.
50. Delgado, J., J. Ciurana, and C.A. Rodríguez, Influence of process parameters on part quality and mechanical properties for DMLS and SLM with iron-based materials. *The International Journal of Advanced Manufacturing Technology*, 2012. 60(5-8): p. 601-610.
51. Regenfuss, P., R. Ebert, and H. Exner, Laser micro sintering—a versatile instrument for the generation of microparts. *Laser Technik Journal*, 2007. 4(1): p. 26-31.
52. Regenfuss, P., et al., Microparts by a novel modification of selective laser sintering. *TECHNICAL PAPERS-SOCIETY OF MANUFACTURING ENGINEERS-ALL SERIES-*, 2004.
53. Aliakbari, E. and H. Baseri, Optimization of machining parameters in rotary EDM process by using the Taguchi method. *The International Journal of Advanced Manufacturing Technology*, 2012. 62(9-12): p. 1041-1053.
54. Udriou, R., *POWDER BED ADDITIVE MANUFACTURING SYSTEMS AND ITS APPLICATIONS*. *Academic journal of manufacturing engineering*, 2012. 10(4).
55. Petrovic, V., et al., Additive layered manufacturing: sectors of industrial application shown through case studies. *International Journal of Production Research*, 2011. 49(4): p. 1061-1079.
56. Saedi, S., et al., Texture, aging, and superelasticity of selective laser melting fabricated Ni-rich NiTi alloys. *Materials Science and Engineering: A*, 2017. 686: p. 1-10.
57. Rahmanian, R., et al. Load bearing and stiffness tailored niti implants produced by additive manufacturing: a simulation study. in *Behavior and Mechanics of Multifunctional Materials and Composites 2014*. 2014. International Society for Optics and Photonics.
58. Jahadakbar, A., et al., Finite element simulation and additive manufacturing of stiffness-matched niti fixation hardware for mandibular reconstruction surgery. *Bioengineering*, 2016. 3(4): p. 36.
59. Dehghanghadikolaei, A., et al., Improving corrosion resistance of additively manufactured nickel–titanium biomedical devices by micro-arc oxidation process. *Journal of materials science*, 2019. 54(9): p. 7333-7355.
60. Moghaddam, N.S., et al. Enhancement of bone implants by substituting nitinol for titanium (Ti-6Al-4V): A modeling comparison. in *Smart Materials, Adaptive Structures and Intelligent Systems*. 2014. American Society of Mechanical Engineers.
61. Dean, H.D., et al., Methods, devices, and manufacture of the devices for musculoskeletal reconstructive surgery. 2017, Google Patents.
62. Hadi, A., et al. Modeling and experiment of a flexible module actuated by shape memory alloy wire. in *Smart Materials, Adaptive Structures and Intelligent Systems*. 2014. American Society of Mechanical Engineers.
63. Raad, B., N.S. Moghaddam, and M. Elahinia. A numerical simulation of the effect of using porous superelastic Nitinol and stiff Titanium fixation hardware on the bone remodeling. in *Nanosensors, Biosensors, and Info-Tech Sensors and Systems 2016*. 2016. International Society for Optics and Photonics.

64. Yadroitsev, I., P. Bertrand, and I. Smurov, Parametric analysis of the selective laser melting process. *Applied surface science*, 2007. 253(19): p. 8064-8069.
65. Moghaddam, N.S., et al., Achieving superelasticity in additively manufactured NiTi in compression without post-process heat treatment. *Scientific reports*, 2019. 9(1): p. 1-11.
66. Elahinia, M., et al., Additive manufacturing of NiTiHf high temperature shape memory alloy. *Scripta Materialia*, 2018. 145: p. 90-94.
67. Ahmadi, A., et al., Effect of manufacturing parameters on mechanical properties of 316L stainless steel parts fabricated by selective laser melting: A computational framework. *Materials & Design*, 2016. 112: p. 328-338.
68. Ma, C., et al., Improving surface finish and wear resistance of additive manufactured nickel-titanium by ultrasonic nano-crystal surface modification. *Journal of Materials Processing Technology*, 2017. 249: p. 433-440.
69. Ibrahim, H., et al., In vitro corrosion assessment of additively manufactured porous NiTi structures for bone fixation applications. *Metals*, 2018. 8(3): p. 164.
70. Esfahani, S.N., et al., Independent tuning of stiffness and toughness of additively manufactured titanium-polymer composites: Simulation, fabrication, and experimental studies. *Journal of Materials Processing Technology*, 2016. 238: p. 22-29.
71. Moghaddam, N.S., et al., Metallic fixation of mandibular segmental defects: Graft immobilization and orofacial functional maintenance. *Plastic and Reconstructive Surgery Global Open*, 2016. 4(9).
72. Moghaddam, N.S., et al., Metals for bone implants: Safety, design, and efficacy. *Biomufacturing Reviews*, 2016. 1(1): p. 1.
73. Saedi, S., et al., On the effects of selective laser melting process parameters on microstructure and thermomechanical response of Ni-rich NiTi. *Acta Materialia*, 2018. 144: p. 552-560.
74. Moghaddam, N.S., et al., Three dimensional printing of stiffness-tuned, nitinol skeletal fixation hardware with an example of mandibular segmental defect repair. *Procedia CIRP*, 2016. 49: p. 45-50.
75. Shayesteh Moghaddam, N., Toward patient specific long lasting metallic implants for mandibular segmental defects. 2015, University of Toledo.
76. Gu, H., et al. Influences of energy density on porosity and microstructure of selective laser melted 17-4PH stainless steel. in 2013 Solid Freeform Fabrication Symposium. 2013.
77. Hu, Z., et al., Experimental investigation on selective laser melting of 17-4PH stainless steel. *Optics & Laser Technology*, 2017. 87: p. 17-25.
78. Irrinki, H., et al., Effects of powder attributes and laser powder bed fusion (L-PBF) process conditions on the densification and mechanical properties of 17-4 PH stainless steel. *Jom*, 2016. 68(3): p. 860-868.
79. Attar, H., et al., Effect of powder particle shape on the properties of in situ Ti–TiB composite materials produced by selective laser melting. *Journal of Materials Science & Technology*, 2015. 31(10): p. 1001-1005.
80. Kumar, S., 10.05 Selective Laser Sintering/Melting In *Comprehensive Materials Processing*; Hashmi, S., Ed. 2014, Elsevier: Amsterdam.
81. Cao, B.X., et al., Design and performance of a focus-detection system for use in laser micromachining. *Micromachines*, 2016. 7(1): p. 2.
82. Hanzl, P., et al., The influence of processing parameters on the mechanical properties of SLM parts. *Procedia Engineering*, 2015. 100(1): p. 1405-1413.
83. Rombouts, M., et al., Fundamentals of selective laser melting of alloyed steel powders. *CIRP annals*, 2006. 55(1): p. 187-192.
84. Yang, Y., et al., Equidistant path generation for improving scanning efficiency in layered manufacturing. *Rapid Prototyping Journal*, 2002.
85. Shi, Y., et al., Compound scan mode developed from subarea and contour scan mode for selective laser sintering. *International Journal of Machine Tools and Manufacture*, 2007. 47(6): p. 873-883.

86. Fernlund, G., et al., Residual stress, spring-in and warpage in autoclaved composite parts. TECHNICAL PAPERS-SOCIETY OF MANUFACTURING ENGINEERS-ALL SERIES-, 2003.
87. Zhang, L.C. and H. Attar, Selective laser melting of titanium alloys and titanium matrix composites for biomedical applications: a review. *Advanced Engineering Materials*, 2016. 18(4): p. 463-475.
88. Ashley, S., Rapid prototyping systems. *Mechanical Engineering*, 1991. 113(4): p. 34.
89. Campbell, R.I., H. Jee, and Y.S. Kim. Adding product value through additive manufacturing. in *DS 75-4: Proceedings of the 19th International Conference on Engineering Design (ICED13), Design for Harmonies, Vol. 4: Product, Service and Systems Design, Seoul, Korea, 19-22.08. 2013.* 2013.
90. Ruffo, M., C. Tuck, and R. Hague, Make or buy analysis for rapid manufacturing. *Rapid Prototyping Journal*, 2007.
91. Thompson, M.K., et al., Design for Additive Manufacturing: Trends, opportunities, considerations, and constraints. *CIRP annals*, 2016. 65(2): p. 737-760.
92. Conner, B.P., et al., Making sense of 3-D printing: Creating a map of additive manufacturing products and services. *Additive Manufacturing*, 2014. 1: p. 64-76.
93. Chua, C.K., et al., Rapid prototyping assisted surgery planning. *The International Journal of Advanced Manufacturing Technology*, 1998. 14(9): p. 624-630.
94. Noorani, R., *Rapid prototyping: principles and applications*. 2006: John Wiley & Sons Incorporated.
95. Flowers, J. and M. Moniz, Rapid prototyping in technology education: rapid prototyping, while costly, can afford students a unique opportunity to bring their ideas to reality. *The Technology Teacher*, 2002. 62(3): p. 7-12.
96. Guo, N. and M.C. Leu, Additive manufacturing: technology, applications and research needs. *Frontiers of Mechanical Engineering*, 2013. 8(3): p. 215-243.
97. Bourell, D.L., M.C. Leu, and D.W. Rosen, Roadmap for additive manufacturing: identifying the future of freeform processing. *The University of Texas at Austin, Austin, TX*, 2009: p. 11-15.
98. Campbell, I., D. Bourell, and I. Gibson, *Additive manufacturing: rapid prototyping comes of age*. *Rapid prototyping journal*, 2012.
99. CNC.FI, Jet Engine bracket SLM.
100. S.A.S., B.A., World Premiere: Brake Caliper from 3D printer. 2018.
101. Steffens A, World's First 3D Printed Hearts And Functional Beating Hearts Grown From Stem Cells. 2019.
102. Lingenfelter, A., Welding of Inconel alloy 718: A historical overview. *Superalloy*, 1989. 718: p. 673-683.
103. Metals, S., Inconel alloy 718. Publication Number SMC-045. Special Metals Corporation, 2007.
104. Çam, G. and M. Koçak, Progress in joining of advanced materials. *International Materials Reviews*, 1998. 43(1): p. 1-44.
105. Liu, F., et al., The effect of laser scanning path on microstructures and mechanical properties of laser solid formed nickel-base superalloy Inconel 718. *Journal of Alloys and Compounds*, 2011. 509(13): p. 4505-4509.
106. Chang, S.-H., In situ TEM observation of  $\gamma'$ ,  $\gamma''$  and  $\delta$  precipitations on Inconel 718 superalloy through HIP treatment. *Journal of alloys and compounds*, 2009. 486(1-2): p. 716-721.
107. MegaMex, Inconer718 Properties.
108. Kuriachen, B. and J. Mathew. MODELING AND MULTI-RESPONSE PREDICTION OF MICRO EDM DRILLING ON INCONEL 718. 2014. All india manufacturing technology, design and research conference.
109. Argen, Mass customizat on comes to dentistry. 2016.
110. Zheng, L., et al., Mechanism of intermediate temperature embrittlement of Ni and Ni-based superalloys. *Critical Reviews in Solid State and Materials Sciences*, 2012. 37(3): p. 181-214.
111. Kuo, C.-M., et al., Aging effects on the microstructure and creep behavior of Inconel 718 superalloy. *Materials Science and Engineering: A*, 2009. 510: p. 289-294.

112. Zhang, Q.-l., J.-h. Yao, and J. Mazumder, Laser direct metal deposition technology and microstructure and composition segregation of Inconel 718 superalloy. *Journal of Iron and Steel Research, International*, 2011. 18(4): p. 73-78.
113. Izquierdo, B., et al., Numerical prediction of heat affected layer in the EDM of aeronautical alloys. *Applied Surface Science*, 2012. 259: p. 780-790.
114. Zheng, L., Z. Maicang, and D. Jianxin, Hot corrosion behavior of powder metallurgy Rene95 nickel-based superalloy in molten NaCl–Na<sub>2</sub>SO<sub>4</sub> salts. *Materials & Design*, 2011. 32(4): p. 1981-1989.
115. Wang, Z., et al., The microstructure and mechanical properties of deposited-IN718 by selective laser melting. *Journal of Alloys and Compounds*, 2012. 513: p. 518-523.
116. Deng, D., *Additively Manufactured Inconel 718: Microstructures and Mechanical Properties*. Vol. 1798. 2018: Linköping University Electronic Press.
117. Rickenbacher, L., et al., High temperature material properties of IN738LC processed by selective laser melting (SLM) technology. *Rapid Prototyping Journal*, 2013.
118. Abe, F., et al., The manufacturing of hard tools from metallic powders by selective laser melting. *Journal of materials processing technology*, 2001. 111(1-3): p. 210-213.
119. Amato, K., et al., Microstructures and mechanical behavior of Inconel 718 fabricated by selective laser melting. *Acta Materialia*, 2012. 60(5): p. 2229-2239.
120. Lu, Z., et al., Review of main manufacturing processes of complex hollow turbine blades: This paper critically reviews conventional and advanced technologies used for manufacturing hollow turbine blades. *Virtual and Physical Prototyping*, 2013. 8(2): p. 87-95.
121. Zhang, Y., et al., Effect of cooling rate on the microstructure of laser-remelted INCONEL 718 coating. *Metallurgical and Materials Transactions A*, 2013. 44(12): p. 5513-5521.
122. Wang, X., X. Gong, and K. Chou, Review on powder-bed laser additive manufacturing of Inconel 718 parts. *Proceedings of the Institution of Mechanical Engineers, Part B: Journal of Engineering Manufacture*, 2017. 231(11): p. 1890-1903.
123. Blackwell, P., The mechanical and microstructural characteristics of laser-deposited IN718. *Journal of materials processing technology*, 2005. 170(1-2): p. 240-246.
124. Zhong, C., et al., Improvement of material performance of Inconel 718 formed by high deposition-rate laser metal deposition. *Materials & Design*, 2016. 98: p. 128-134.
125. Trosch, T., et al., Microstructure and mechanical properties of selective laser melted Inconel 718 compared to forging and casting. *Materials letters*, 2016. 164: p. 428-431.
126. Jiang, J., X. Xu, and J. Stringer, Support structures for additive manufacturing: a review. *Journal of Manufacturing and Materials Processing*, 2018. 2(4): p. 64.
127. Kruth, J.-P., et al., Selective laser melting of iron-based powder. *Journal of materials processing technology*, 2004. 149(1-3): p. 616-622.
128. Cloots, M., A. Spierings, and K. Wegener. Assessing new support minimizing strategies for the additive manufacturing technology SLM. in *Solid freeform fabrication symposium*. 2013.
129. Gan, M.X. and C.H. Wong, Practical support structures for selective laser melting. *Journal of Materials Processing Technology*, 2016. 238: p. 474-484.
130. Hussein, A., et al., Advanced lattice support structures for metal additive manufacturing. *Journal of Materials Processing Technology*, 2013. 213(7): p. 1019-1026.
131. Jhabvala, J., et al., An innovative method to build support structures with a pulsed laser in the selective laser melting process. *The International Journal of Advanced Manufacturing Technology*, 2012. 59(1-4): p. 137-142.
132. Vandenbroucke, B. and J.P. Kruth, Selective laser melting of biocompatible metals for rapid manufacturing of medical parts. *Rapid Prototyping Journal*, 2007.
133. Buican, G.R., G. Oancea, and R.F. Martins. Study on SLM manufacturing of teeth used for dental tools testing. in *MATEC Web of Conferences*. 2017. EDP Sciences.
134. Papadakis, L., et al. Numerical modeling of heat effects during thermal manufacturing of aero engine components. in *Proceedings of the World Congress on Engineering*. 2012.

135. Thomas, D., Costs, benefits, and adoption of additive manufacturing: a supply chain perspective. *The International Journal of Advanced Manufacturing Technology*, 2016. 85(5-8): p. 1857-1876.
136. Lindemann, C., et al. Analyzing product lifecycle costs for a better understanding of cost drivers in additive manufacturing. in *23th Annual International Solid Freeform Fabrication Symposium—An Additive Manufacturing Conference*. Austin Texas USA 6th-8th August. 2012.
137. Khajavi, S.H., J. Partanen, and J. Holmström, Additive manufacturing in the spare parts supply chain. *Computers in industry*, 2014. 65(1): p. 50-63.
138. Li, F., Automated cost estimation for 3-axis CNC milling and stereolithography rapid prototyping. 2012.
139. Allen, J., An investigation into the comparative costs of additive manufacture vs. machine from solid for aero engine parts. 2006, *ROLLS-ROYCE PLC DERBY (UNITED KINGDOM)*.
140. Baumers, M., Economic aspects of additive manufacturing: benefits, costs and energy consumption. 2012, *Loughborough University*.
141. Gibson, I., D.W. Rosen, and B. Stucker, *Additive manufacturing technologies*. Vol. 17. 2014: Springer.
142. Rickenbacher, L., A. Spierings, and K. Wegener, An integrated cost-model for selective laser melting (SLM). *Rapid Prototyping Journal*, 2013.
143. 3D Systems, *3D Additive Manufacturing Software*.
144. 3D Systems Middle East and North Africa, *Materialize Magics*.
145. Siemens, *Atlas 3D*.
146. Siemens, *3D printing*.
147. Järvinen, J.-P., et al., Characterization of effect of support structures in laser additive manufacturing of stainless steel. *Physics Procedia*, 2014. 56: p. 72-81.
148. Harris, J., R. Winter, and G.J. McShane, Impact response of additively manufactured metallic hybrid lattice materials. *International Journal of Impact Engineering*, 2017. 104: p. 177-191.
149. Materialise, “Three Big Benefits Provided by Optimal Metal Supports.”
150. Cantrell, J.T., et al., Experimental characterization of the mechanical properties of 3D-printed ABS and polycarbonate parts. *Rapid Prototyping Journal*, 2017.
151. Mirzendehtel, A.M. and K. Suresh, Support structure constrained topology optimization for additive manufacturing. *Computer-Aided Design*, 2016. 81: p. 1-13.
152. Langelaar, M., Topology optimization of 3D self-supporting structures for additive manufacturing. *Additive Manufacturing*, 2016. 12: p. 60-70.
153. Wang, D., et al., Research on the fabricating quality optimization of the overhanging surface in SLM process. *The International Journal of Advanced Manufacturing Technology*, 2013. 65(9-12): p. 1471-1484.
154. Mertens, R., et al., Optimization of scan strategies in selective laser melting of aluminum parts with downfacing areas. *Journal of Manufacturing Science and Engineering*, 2014. 136(6).
155. Kranz, J., D. Herzog, and C. Emmelmann, Design guidelines for laser additive manufacturing of lightweight structures in TiAl6V4. *Journal of Laser Applications*, 2015. 27(S1): p. S14001.
156. Strano, G., et al., A new approach to the design and optimisation of support structures in additive manufacturing. *The International Journal of Advanced Manufacturing Technology*, 2013. 66(9-12): p. 1247-1254.
157. Vanek, J., J.A.G. Galicia, and B. Benes. Clever support: Efficient support structure generation for digital fabrication. in *Computer graphics forum*. 2014. Wiley Online Library.
158. Calignano, F., Design optimization of supports for overhanging structures in aluminum and titanium alloys by selective laser melting. *Materials & Design*, 2014. 64: p. 203-213.
159. ImageJ, R.W., ImageJ, R.W., *US Natl Institutes Heal Bethesda, Maryland, USA*. 2012. .
160. Sanviemvongsak, T., D. Monceau, and B. Macquaire, High temperature oxidation of IN 718 manufactured by laser beam melting and electron beam melting: Effect of surface topography. *Corrosion Science*, 2018. 141: p. 127-145.

161. Biscuola, V. and M. Martorano, Mechanical blocking mechanism for the columnar to equiaxed transition. *Metallurgical and Materials Transactions A*, 2008. 39(12): p. 2885-2895.
162. Mignanelli, P., et al., Gamma-gamma prime-gamma double prime dual-superlattice superalloys. *Scripta Materialia*, 2017. 136: p. 136-140.